# Experimental Investigation of the NASA Common Research Model (Invited)

Melissa B. Rivers[*]
*NASA Langley Research Center, Hampton, VA 23681*

Ashley Dittberner[†]
*Jacobs Sverdrup, Hampton, VA 23681*

An experimental aerodynamic investigation of the NASA Common Research Model has been conducted in the NASA NTF (National Transonic Facility). Data have been obtained at chord Reynolds numbers of 5, 19.8 and 30 million for the WB and WBT0 configurations. Data have also been obtained at a chord Reynolds number of 5 million for the WBNP, WBT+2 and WBT-2 configurations. Force and moment, surface pressure and surface flow visualization data were obtained but only the force and moment data are presented herein. Model deformation measurements, aeroelastic, nacelle/pylon, Reynolds number and tail effects have been assessed. The model deformation measurements showed more twist as you go out the wing span, with a break in the high $q_\infty$ data close to $C_L = 0.6$ which is consistent with separation near the tip. Increases in dynamic pressure give an increase in pitching moment and drag and a decrease in lift for the WB and WBT0 configuration at Mach = 0.7, 0.85 and 0.87. The addition of a nacelle/pylon gave an increase in drag, decrease in lift and a less nose down pitching moment around the design lift condition of 0.5. Increases in chord Reynolds number have been found to follow the normal Reynolds number trends except at the 19.8 million low $q_\infty$ cases. The abnormality of the 19.8 million low $q_\infty$ cases is still under investigation. The tail effects also follow the expected trends. Finally, all of the data shown fall within the 2-sigma limits for repeatability.

## Nomenclature

| | | |
|---|---|---|
| b | = | wing span, in. |
| c | = | wing mean aerodynamic chord, in. |
| $C_D$ | = | drag coefficient |
| $C_L$ | = | lift coefficient |
| $C_m$ | = | pitching moment coefficient referenced to 0.25 of the wing mean aerodynamic chord |
| $C_p$ | = | pressure coefficient |
| CFD | = | computational fluid dynamics |
| CRM | = | Common Research Model |
| DPW | = | Drag Prediction Workshop |
| $M_\infty$ | = | freestream Mach number |
| NASA | = | National Aeronautics and Space Administration |

---

[*] Research Engineer, Configuration Aerodynamics Branch, Mail Stop 267, Senior Member AIAA
[†] Test Engineer, ROME Group, Mail Stop 267, Senior Member AIAA

| NTF | = | National Transonic Facility |
|---|---|---|
| $q_\infty$ | = | dynamic pressure, psf |
| $Re_c$ | = | Reynolds number based on mean aerodynamic chord |
| S | = | model reference area, ft$^2$ |
| WB | = | Wing/Body |
| WBNP | = | Wing/Body/Nacelle/Pylon |
| WBT0 | = | Wing/Body/Tail=0º |
| WBT+2 | = | Wing/Body/Tail=+2º |
| WBT-2 | = | Wing/Body/Tail=-2º |
| x/c | = | longitudinal distance from wing leading edge nondimensionalized by local wing chord |
| $\alpha$ | = | angle of attack, deg |
| $\theta$ | = | wing twist angle, deg |
| $\eta$ | = | fraction of wing semi-span |

# I.  Introduction

In an effort to assess the state of the art in computational fluid dynamics (CFD) drag prediction, the AIAA Applied Aerodynamics Technical Committee has initiated a series of Drag Prediction Workshops. The goal of the workshops is to assess state-of-the-art computational methods as practical aerodynamic tools for aircraft force and moment prediction of industry relevant geometries, with the focus being on drag prediction. The Drag Prediction Workshops (DPW) are designed to serve as an impartial forum for evaluating the effectiveness of existing computational Navier-Stokes solvers and modeling techniques. In addition, the DPW forum is intended to promote an open discussion on areas needing additional research and development. In order to encourage the widest participation, public-domain subject geometries have been used that are industry-relevant, yet simple enough to permit high-fidelity computations. Additionally, baseline grids have been provided with the intent of reducing the variability of CFD results.

The first drag prediction workshop[1,2] (DPW-I), held in June of 2001, was directed at the calculation of a wing/body commercial transport configuration, known as the DLR-F4[3,4]. Previously obtained experimental data were used as a reference for this first workshop. Predictions of a cruise polar and the drag rise were the focus. The second drag prediction workshop[5,6] (DPW-II), held in June of 2003, added the challenge of determining the increment due to adding a large component, in this case a pylon/nacelle. The DLR-F6 configuration[5,7] was used for this study. Once again, experimental data were available for comparison. The third drag prediction workshop[8,9] (DPW-III), held in June of 2006, added the challenge of determining the increment due to adding a small component, in this case a wing/body fairing. However for this workshop, the calculations were conducted "blind" with no experimental data available prior to the workshop. Force and moment, surface pressure, model deformation, and surface flow visualization data were obtained in an NTF wind tunnel investigation on the DLR-F6 configuration in the fall of 2007[10]. The fourth drag prediction workshop (DPW-IV), held in June of 2009, was another set of blind calculations. However for this workshop, the calculations were conducted on a brand new model called the Common Research Model (CRM). It is these "blind" calculations that draw the connection between the fourth drag prediction workshop and the current experimental investigation. The force and moment, surface pressure, model deformation, and surface flow visualization data obtained in an NTF wind tunnel investigation on the CRM and the results presented in this paper serve as the validation data for the calculations presented in the DPW-IV.

# II.  Experimental Approach

## A.  Facility Description

The NTF[11] is a unique national facility (Figure 1) that enables testing of aircraft configurations at conditions ranging from subsonic to low supersonic speeds at Reynolds numbers up to full-scale flight values. The NTF is a conventional, closed circuit, continuous-flow, fan-driven, pressurized wind tunnel (Figure 2) capable of operating in either dry air at warm temperatures or nitrogen from warm to cryogenic temperatures. Elevated pressures in combination with cryogenic temperatures enable testing to the highest Reynolds numbers. The test section is 8.2 by 8.2 by 25 ft and has a slotted floor and ceiling. In addition, four damping screens in the settling chamber and a contraction ratio of 14.95-to-1 reduce turbulence from the settling chamber to the nozzle throat. Fan-noise effects are minimized by acoustic treatment both upstream and downstream of the fan. Thermal insulation resides inside the pressure shell to aid in maintaining tunnel temperature and thus minimize energy consumption.

The NTF has an operating pressure range of approximately 15 to 125 psia, a temperature range of -260 to +120°F, and a Mach number range of 0.2 to 1.2. The maximum Reynolds number per foot is 146 x $10^6$ at Mach 1. When the tunnel is operated cryogenically, heat is removed by the evaporation of liquid nitrogen, which is sprayed into the tunnel circuit upstream of the fan. During this operational mode, venting is necessary to maintain a constant total pressure. When air is the test gas, heat is removed from the system by a water-cooled heat exchanger at the upstream end of the settling chamber. A mixed mode of operation can be used to reach higher Reynolds numbers. This mode uses liquid nitrogen to augment the cooling coil without the expense of fully crossing over into nitrogen mode. Further tunnel details and facility information are provided in Ref. 12.

## B.  Model Description

The model used in the current investigation was the NASA Common Research Model (CRM).  This configuration consists of a contemporary supercritical transonic wing and a fuselage that is representative of a wide-body commercial transport aircraft.  The CRM is designed for a cruise Mach number of $M_\infty = 0.85$ and a corresponding design lift coefficient of $C_L = 0.5$.  A sketch of the CRM with reference quantities listed is shown in Figure 3.  The aspect ratio is 9.0, the leading edge sweep angle is 35 deg, the wing reference area (S) is 3.01 $ft^2$, the wing span (b) is 62.46 inches, and the mean aerodynamic chord (c) is 7.45 inches.  The model moment reference center is located 35.8 inches back from the fuselage nose and 2.04 inches below the fuselage centerline. The nacelles used for this test were simple, flow through nacelles. Pressure distributions are measured on both the left and right wings using 291 pressure orifices located in 9 span-wise wing stations ($\eta$ = 0.131, 0.201, 0.283, 0.397, 0.502, 0.603, 0.727, 0.846, and 0.950) and on the left hand nacelle by 6 orifices at 6 radial stations ($\eta = 30^o, 90^o, 150^o, 210^o, 270^o,$ and $330^o$). All pressure measurements were made using Electronically Scanned Pressure (PSP) modules mounted inside the forward portion of the fuselage.  Based on quoted accuracies from the ESP module manufacturer, surface pressure measurements should be in error no more than +/- 0.015 psi.  This in turn would correspond to a variation of no more than +/- 0.0026 in terms of Cp.  The pressure measurements from this investigation are not presented herein but will be presented in a future publication. The model is mounted in the wind tunnel using a blade sting arrangement as shown in fig. 4.  No corrections have been made for this mounting arrangement.

Five different configurations were tested in the current investigation: the wing/body (WB) alone, wing/body/nacelle/pylon (WBNP), wing/body/tail=0° (WBT0), wing/body/tail=+2° (WBT+2) and wing/body/tail=-2° (WBT-2).  Further details on this geometry are given in Ref. 13.

## C.  Test Conditions

The investigation, conducted over a 6-week period, provided force and moment, surface pressure, model deformation, and surface flow visualization data.  Testing was conducted at 5, 19.8 and 30 million Reynolds number.  The 5 and 19.8 million Reynolds number data were collected to provide a comparison to previously calculated CFD results and all of the Reynolds numbers were used to provide an assessment of Reynolds number effects. The 19.8 million Reynolds number data were collected at two different $q_\infty$ levels – a high and a low $q_\infty$ condition.  Having two $q_\infty$ levels at the same Reynolds number provides an aeroelastic step in the data. All Reynolds number values presented in this paper are based on mean aerodynamic chord.  The data were collected at temperatures ranging from -250ºF up to 120º F.

All data presented in this paper were obtained at freestream Mach numbers ranging from 0.7 to 0.87. Data were generally obtained over an angle-of-attack range from -3° to +12° at 5 million Reynolds number and from -3° to +6° at 19.8 and 30 million Reynolds numbers. The reduced angle-of-attack range at the higher Reynolds number was required such that safe model stress levels would not be exceeded. Flow angularity measurements were made and upflow corrections ranging from 0.092° to 0.173° were applied to the final data. Classical wall corrections accounting for model blockage, wake blockage, tunnel buoyancy, and lift interference have been applied according to the methods presented in Ref. 14. Testing on the WBNP, WBT+2 and WBT-2 configurations was conducted at a Reynolds number of 5 million only. However, data were obtained at all three Reynolds numbers for both the WB and WBT0 configurations.

In order to ensure a consistent and repeatable transition from laminar to turbulent flow and to support the goal of the wind tunnel data being used for CFD validation purposes, it was important to apply a proven and reliable method to fix transition on the model. Evercoat trip dots measuring 0.05 inches in diameter and spaced 0.1 inches apart (center to center) were used for the current investigation. For a Reynolds number of 5 million, a trip dot height of 0.0035 inches was used from the SOB (side of body) to the yehudi break, 0.0045 inches was used from the yehudi break to the midwing and 0.004 inches was used from the midwing to the wing tip. These trip dots were installed at 10% chord.  Vinyl adhesive trip dots were applied at the nose of the fuselage and left on for the entire test. When the

nacelles were on the model, trip dots were located 0.43 inches back from the leading edge on the outer surface and the inner surface. Finally, when the tails were on the model, trip dots were located at 10% chord and measured 0.003 inches.

Another important set of data obtained in this investigation was model deformation measurements. Since an effective correlation of computational and experimental data will be directly tied to how well the computational and experimental model geometries match one another, it is important to obtain an accurate definition of the model geometry as tested under aerodynamic loads. In order to obtain this information a video model deformation measurement technique[15] has been developed and employed multiple times at the NTF. This system was used in the current investigation to obtain wing deflection and twist measurements due to aerodynamic loading.

## III.  Results and Discussion

### A.  Model Deflection Measurements
Figures 5-8 show the aeroelastic twist vs. $C_L$ at Mach 0.85 for the 5 positions on the wing measured during the test.  These 4 figures are for the WBT0 configuration at $Re_c$=5 million-low $q_\infty$, 19.8 million-low $q_\infty$, 19.8 million-high $q_\infty$, and 30 million-high $q_\infty$.  The high $q_\infty$ data (figures 7-8) have a distinct break close to $C_L$=0.6, consistent with separation near the tip.

Figure 9 shows the data from figs. 5-8 at the $\eta = 0.7272$ location to compare the effects of Reynolds number and $q_\infty$.  The 19.8 million and 30 million Reynolds number data were taken at nearly the same $q_\infty$ value but the 30 million data has more negative twist.  This may due in part to variability.  However, the shock moves aft and the aft loading increases at higher Reynolds numbers, which increase the nose down moment, consistent with the twist data trend.

Figure 10 shows the $\eta = 0.7272$ data for the WB alone configuration.  At the high $q_\infty$ conditions, there is not as much difference between high and low Reynolds number at the higher $C_L$ values as there was for the WBT0 configuration.

### B.  Aeroelastic effects
One goal of the current investigation was to determine aeroelastic effects on this new configuration.  Figures 11 – 16 show the aeroelastic effects for both the WB and WBT0 configurations at Mach = 0.7, 0.85 and 0.87 with the aeroelastic step being taken at 19.8 million Reynolds number.  In these figures, a close up view of the plots are given on the right hand side of the figure.  Fig. 11 shows that for WB at Mach 0.7, an increase in $q_\infty$ gives a higher $C_D$ value, a lower $C_L$ and a less nose down pitching moment.  Figure 12 indicates that for the WBT0 configuration the same trends exist as the WB configuration.  Figs. 13 and 14 show the aeroelastic effects for WB and WBT0 configurations at Mach 0.85.  Again, an increase in $q_\infty$ gives a higher $C_D$ value, a lower $C_L$ and less nose down pitching moment for both configurations.  Finally, figs. 15 and 16 show that for WB and WBT0 at Mach 0.87, an increase in $q_\infty$ gives a higher $C_D$ value, a lower $C_L$ and less nose down pitching moment for both configurations.

### C.  Nacelle/Pylon effects
Determining the effects of adding a nacelle/pylon to the configuration were another goal of the current investigation.  Figures 17 – 19 show these effects at Mach 0.7, 0.85 and 0.87, respectively.  Figure 17 indicates that at Mach 0.7, the addition of a nacelle/pylon increases the drag, lowers the lift and gives a less nose down pitching moment at $C_L = 0.5$.  In fig. 18 it is shown that the drag again increases, the lift again lowers and the pitching moment is again less nose down at $C_L = 0.5$ and Mach = 0.85 with the addition of a nacelle/pylon.  Finally, fig. 19 shows that for a Mach number of 0.87, the drag increases, the lift decreases and the pitching moment is less nose down for a $C_L = 0.5$ with a nacelle/pylon added.

### D.  Reynolds Number Effects
Another goal of the current investigation was to establish a database for Reynolds numbers from 5 million up to 30 million such that an assessment of Reynolds number effects could be made. Data have been obtained at 5, 19.8 and 30 million Reynolds number at three different Mach numbers for the WB and WBT0 configurations, and these data are presented in figs. 20 – 25.

Figure 20 shows the Reynolds number effects for the WB configuration at Mach 0.7 and fig. 21 shows the Reynolds number effects for the WBT0 configuration at Mach 0.7. Upon examination of the lift coefficient data for these two data sets, it would appear there is essentially no Reynolds number effect, except for the low $q_\infty$ 19.8 million case. However, Reynolds number effects are clearly seen for both drag and pitching moment. In general, for a constant angle of attack, an increase in Reynolds number primarily leads to an increase in lift due to a thinner

boundary layer and thus an increased effective camber of the wing. In the current data set however, increased Reynolds number comes along with increased dynamic pressure and in turn static aeroelastic effects. Aeroelastic effects due to the increased dynamic pressure at the 19.8 and 30 million Reynolds number result in an increased nose-down wing twist, which would in turn act to reduce lift. Thus the lack of any noticeable Reynolds number effect on the lift coefficient data presented is likely due to offsetting Reynolds number and static aeroelastic effects. This trend of offsetting Reynolds number and static aeroelastic effects has been encountered in previous investigations in the NTF and is documented in Ref. 16.

As Reynolds number is increased, a reduction in drag is noted for both configurations from 5 to 30 million Reynolds number but the 19.8 million low $q_\infty$ cases do not fit this trend; the drag increases from the 19.8 low $q_\infty$ to the 19.8 high $q_\infty$ case. In addition, as Reynolds number is increased there is an increase in nose-down pitching moment except at the 19.8 million low $q_\infty$ case, with this increment in nose-down pitching moment being much larger than the other Reynolds numbers.

Figures 22 and 23 show the Reynolds number effects for the WB and WBT0 configurations, respectively, at Mach 0.85. The lift coefficients at this Mach number for the WB configuration does show an increase in lift with an increase in Reynolds number, except for the low $q_\infty$ 19.8 million case, which is showing the higher lift values than the 30 million Reynolds number data. For the WBT0 configuration, little Reynolds number effects are seen except for the low $q_\infty$ 19.8 million case. As seen in the Mach 0.7 cases, a reduction in drag is noted for both configurations from 5 to 30 million Reynolds number but the 19.8 million low $q_\infty$ cases do not fit this trend, as the 19.8 low $q_\infty$ data seems to fall right on top of the 30 million data. In addition, as Reynolds number is increased there is an increase in nose-down pitching moment for the WB configuration except at the 19.8 million low $q_\infty$ case, which shows a greater nose down pitching moment than the 30 million Reynolds number data. For the WBT0 configuration, little to no Reynolds number effect is seen for the pitching moment except for the low $q_\infty$ 19.8 million Reynolds number case, which shows a much larger nose down pitching moment than the other Reynolds numbers.

Finally, figs. 24 and 25 show the Reynolds number effects for the WB and WBT0 configurations, respectively, at Mach 0.87. The results for this Mach number show that the lift coefficients at this Mach number do show an increase in lift with an increase in Reynolds number, except for the low $q_\infty$ 19.8 million case; a reduction in drag is noted for both configurations from 5 to 30 million Reynolds number but the 19.8 million low $q_\infty$ cases do not fit this trend due to the drag increasing from the 19.8 low $q_\infty$ to the 19.8 high $q_\infty$ case. In addition, as Reynolds number is increased there is an increase in nose-down pitching moment except at the 19.8 million low $q_\infty$ case, which shows a much larger nose down pitching moment than the other Reynolds numbers.

**E.  Tail Effects**

Another goal of this investigation was to determine the tail effects for this configuration. Three different tail settings were tested – tail = -2º, tail = +2º and tail = 0º, on the wing/body configuration. All of these cases were run at a Reynolds number of 5 million. Figures 26 – 28 show the tail effects for Mach = 0.7, 0.85 and 0.87, respectively. In fig. 26 we see that going from a -2º to a +2º tail setting shows little to no change in drag, gives an increase in lift and gives an increase in nose-down pitching moment, as expected, for the Mach 0.7 condition. Fig. 27 shows that for the Mach = 0.85 condition, there is a decrease in drag, increase in lift and an increase in nose down pitching moment when going from a -2º to a +2º tail setting. This same trend is also seen for the Mach = 0.87 case in fig. 28.

**F.  Data Repeatability**

When data are obtained in any experimental investigation it is important to make an assessment of data accuracy or data repeatability. In order to make such an assessment for the current investigation, multiple repeat runs were obtained for both the WB and WBT0 configurations. To obtain the most reliable assessment of data repeatability it is best to have the repeat runs distributed widely throughout the duration of the investigation. Unfortunately this process is usually in conflict with an efficient execution of the test plan. Keeping these thoughts in mind, the following sets of repeat runs were obtained. Within each series of runs, 3 runs were obtained at $M_\infty = 0.7, 0.85$ and 0.87 and at all three Reynolds number. Each of these 3 runs were always separated by at least one run at a different test condition. This resulted in 3 repeat runs for the all of the configurations at all of the conditions listed above. The repeatability data resulting from these runs are presented in figs. 29 - 36. Delta coefficient data are presented versus angle of attack for each configuration at each condition. The delta coefficient data presented represent the difference between the coefficient value measured and the average value of the coefficient at that particular angle of attack. These delta coefficient, or residual, data show the level of variation in the repeat runs. The solid lines shown on each

plot indicate the 2-sigma limits based on all the data across the angle-of-attack range. Thus it is shown that essentially all the residual data fall within the 2-sigma limits.

## IV.  Summary

A successful investigation of the new NASA Common Research Model has been completed in the National Transonic Facility.  Data have been obtained at chord Reynolds numbers of 5, 19.8 and 30 million for the WB and WBT0 configurations.  Data have also been obtained at a chord Reynolds number of 5 million for the WBNP, WBT+2 and WBT-2 configurations.  Force and moment, surface pressure and surface flow visualization data were obtained but only the force and moment data are presented herein.  Model deformation measurements, aeroelastic, nacelle/pylon, Reynolds number and tail effects have been assessed.

1) The model deformation measurements showed more twist as you go out the wing span, with a break in the high $q_\infty$ data close to $C_L = 0.6$ which is consistent with separation near the tip.
2) Increases in dynamic pressure give an increase in pitching moment and drag and a decrease in lift for the WB and WBT0 configuration at Mach = 0.7, 0.85 and 0.87.
3) The addition of a nacelle/pylon gave an increase in drag, decrease in lift and a less nose down pitching moment around the design lift condition of 0.5.
4) Increases in chord Reynolds number have been found to follow the normal Reynolds number trends except at the 19.8 million low $q_\infty$ cases.  The abnormality of the 19.8 million low $q_\infty$ cases is being investigated.
5) The tail effects also follow the expected trends.
6) All of the data shown fall within the 2-sigma limits for repeatability.

## Acknowledgments

# References

[1] Levy, D. W., Vassberg, J. C., Wahls, R. A., Zickhur, T., Agrawal, S., Pirzadeh, S., and Hemsch, M. J., "Summary of Data from the First AIAA CFD Drag Prediction Workshop," AIAA Paper 2002-0841, January 2002.

[2] Hemsch, M. J., "Statistical Analysis of CFD Solutions from the Drag Prediction Workshop," AIAA Paper 2002-0842, January 2002.

[3] Redeker, G., Schmidt, N., and Muller, R., "Design and Experimental Verification of a Transonic Wing for a Transport Aircraft," *Proceedings of the FDP Symposium on Subsonic/Transonic Configuration Aerodynamics*, AGARD CP 285, 1980, pp. 13.1-13.7.

[4] Redeker, G., "DLR-F4 Wing Body Configuration," *A Selection of Experimental Test Cases for the Validation of CFD Codes*, AGARD Report AR-303, Vol. 2, 1994, pp. B4-1-21.

[5] Laflin, K. R., Vassberg, J. C., Wahls, R. A., Morrison, J. H., Brodersen, O., Radowitz, M., Tinoco, E. N., and Godard, J., "Summary of Data from the Second AIAA CFD Drag Prediction Workshop," AIAA Paper 2004-0555, January 2004.

[6] Hemsch, M. J. and Morrison, J. H., "Statistical Analysis of CFD Solutions from the 2nd Drag Prediction Workshop," AIAA Paper 2004-0556, January 2004.

[7] Rossow, C.-C., Godard, J.-L., Hoheisel, H., and Schmitt, V., "Investigations of Propulsion Integration Interference Effects on a Transport Aircraft Configuration," *Journal of Aircraft*, Vol. 31, No. 5, 1994, pp. 1022-1030.

[8] Vassberg, J. C., Tinoco, E. N., Mani, M., Broderson, O. P., Eisfeld, B., Wahls, R. A., Morrison, J. H., Zickuhr, T., Laflin, K. R., and Mavriplis, D. J., "Summary of the Third AIAA CFD Drag Prediction Workshop," AIAA Paper 2007-0260, January 2007.

[9] Morrison, J. H. and Hemsch, M. J., "Statistical Analysis of CFD Solutions from the Third AIAA Drag Prediction Workshop," AIAA Paper 2007-0254, January 2007.

[10] Gatlin, G. M., Rivers, M.B., Goodliff, S. L., Rudnik, R., and Sitzmann, M., "Experimental Investigation of the DLR-F6 Transport Configuration in the National Transonic Facility (invited)," AIAA Paper 2008-6917, August 2008.

[11] Gloss, B. B., "Current Status and Some Future Test Directions for the US National Transonic Facility. Wind Tunnels and Wind Tunnel Test Techniques," *Royal Aeronautical Society*, 1992, pp. 3.1-3.7.

[12] Fuller, D. E., "Guide for Users of the National Transonic Facility," NASA TM-83124, 1981.

[13] J. C. Vassberg, M. A. DeHaan, S. M. Rivers, and R. A. Wahls. Development of a Common Research Model for Applied CFD validation studies. AIAA Paper 2008-6919, 26th AIAA Applied Aerodynamics Conference, Hawaii, HI, August 2008.

[14] Iyer, V., "A Wall Correction Program Based on Classical Methods for the National Transonic Facility (Solid Wall or Slotted Wall) and the 14x22-Ft Subsonic Tunnel at NASA LaRC." NASA/CR-2004-213261, October 2004.

[15] Burner, A. W. and Liu, T., "Videogrammetric Model Deformation Measurement Technique," *Journal of Aircraft*, Vol. 38, No. 4, July-August 2001, pp. 745-754.

[16] Wahls, R. A., Gloss, B. B., Flechner, S. G., Johnson, W. G., Jr., Wright, F. L., Nelson, C. P., Nelson, R. S., Elzey, M. B., and Hergert, D. W., "A High Reynolds Number Investigation of a Commercial Transport Model in the National Transonic Facility," NASA TM-4418, 1993.

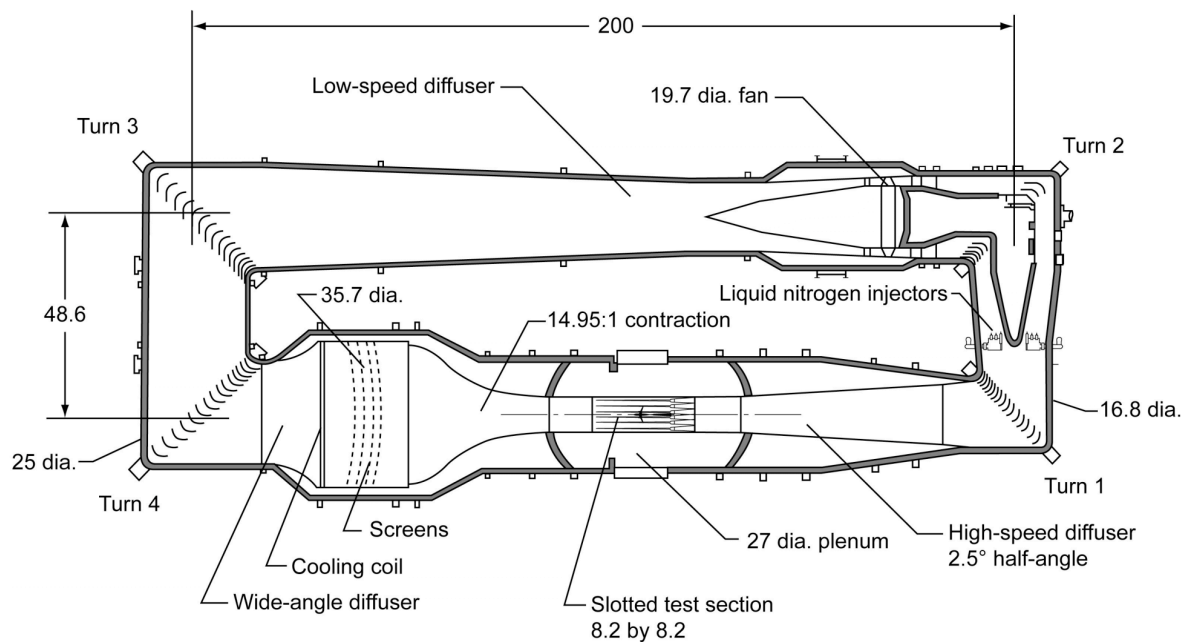**Figure 1. Aerial View of the National Transonic Facility.**



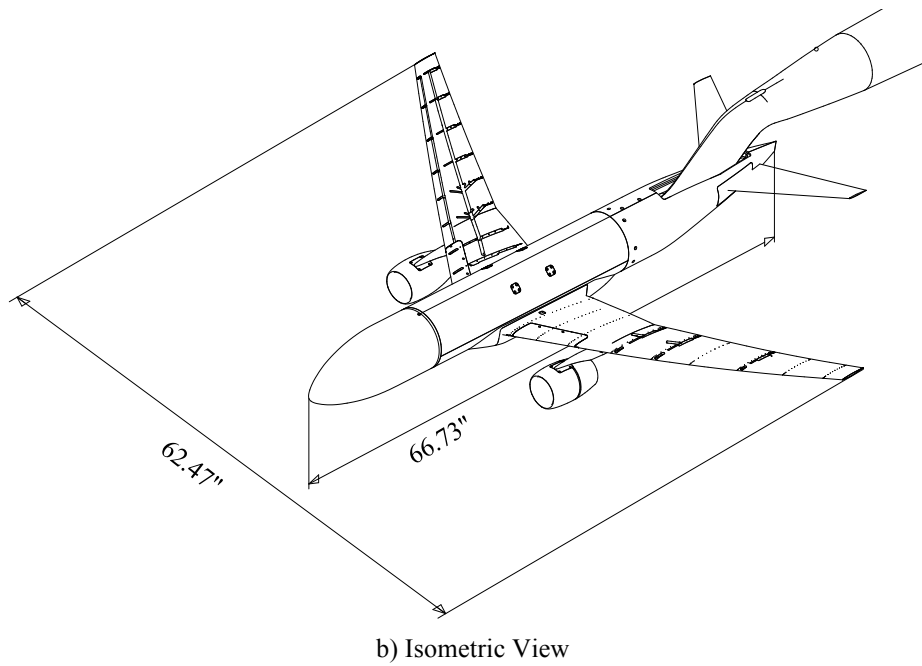**Figure 2. Sketch of the National Transonic Facility tunnel circuit. Linear dimensions are given in feet.**
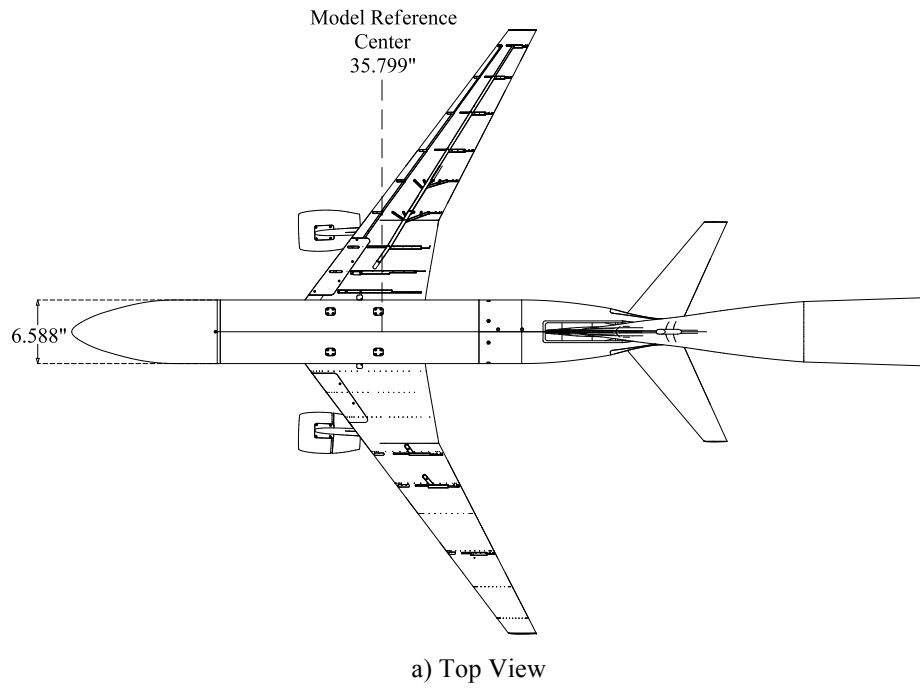
American Institute of Aeronautics and Astronautics

NTF

Model Reference
Center
35.799"

6.588"

a) Top View

NTF

62.47"

66.73"

b) Isometric View

**Figure 3. Sketch of the Common Research Model with Reference Quantities.**

American Institute of Aeronautics and Astronautics
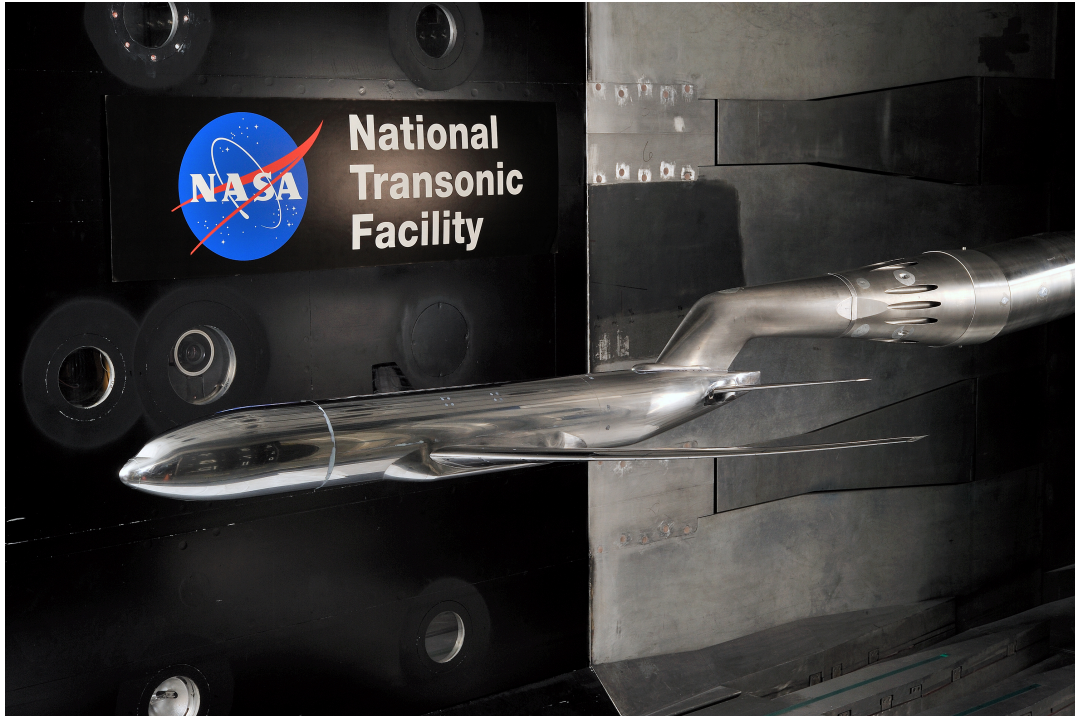
**Figure 4. Photo of the Common Research Model in the National Transonic Facility.**



| Config | Tail ∠θ | $q_\infty$,psf | ηθ |
|--------|---------|----------|------|
| WBT | 0° | 1388. | 0.000 |
| WBT | 0° | 1388. | 0.2765 |
| WBT | 0° | 1388. | 0.4481 |
| WBT | 0° | 1388. | 0.5576 |
| WBT | 0° | 1388. | 0.7272 |
| WBT | 0° | 1388. | 0.9464 |

**Figure 5. Model Deformation, WBT0 Configuration, Mach = 0.85, $Re_c$ = 5x10$^6$, low $q_\infty$.**

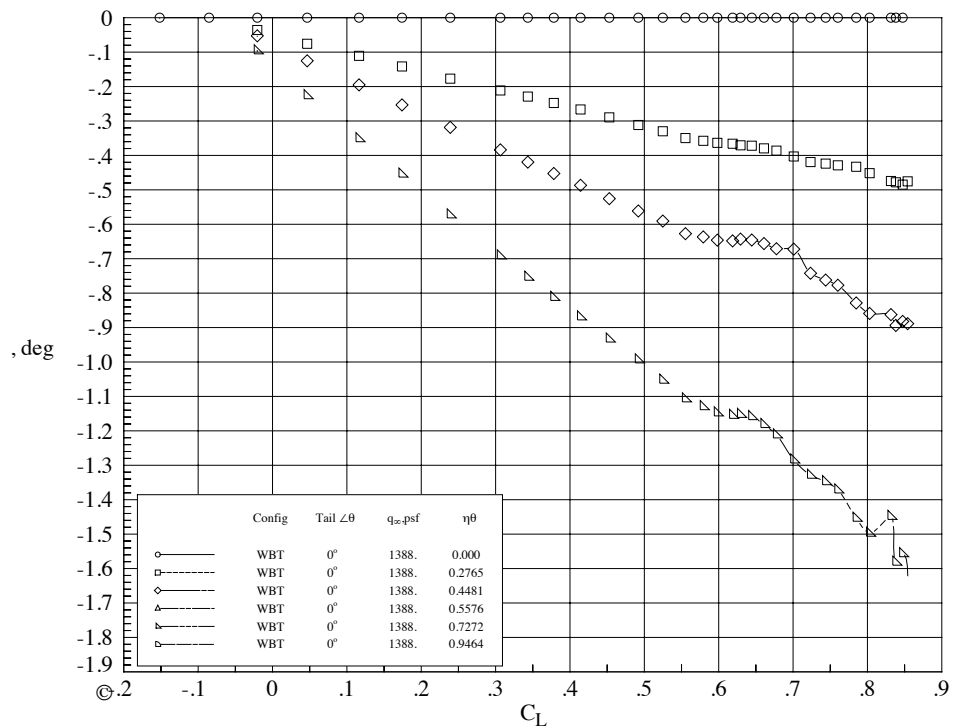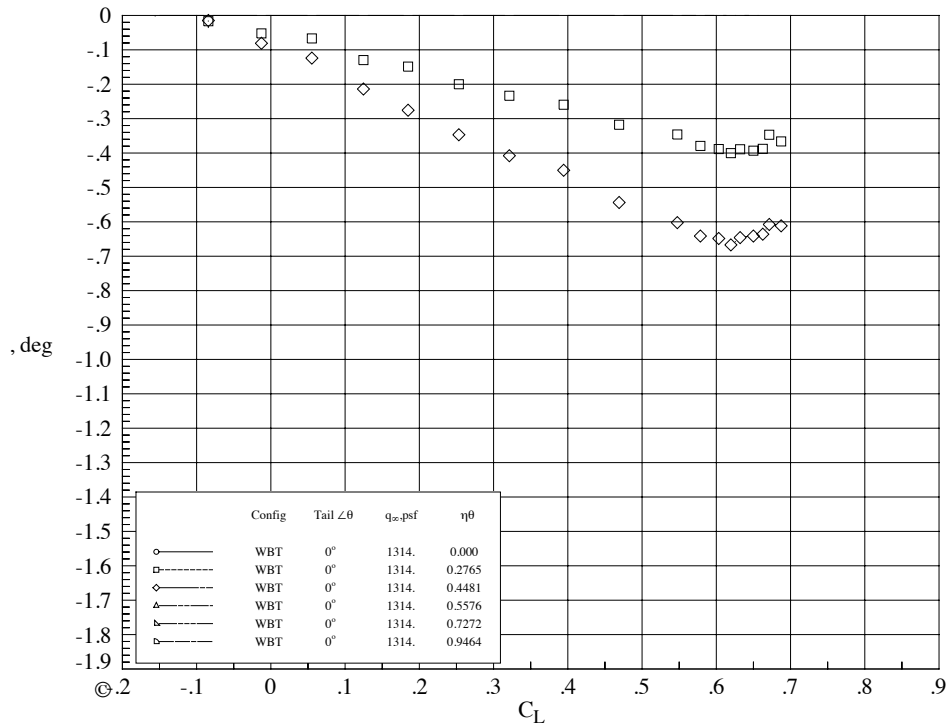American Institute of Aeronautics and Astronautics
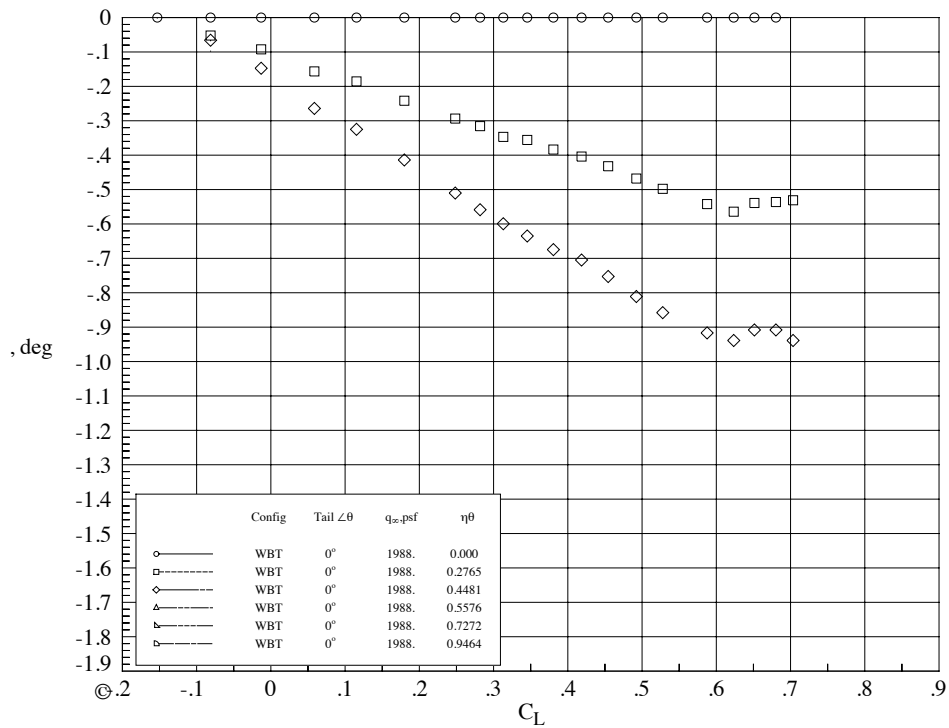
**Figure 6. Model Deformation, WBT0 Configuration, Mach = 0.85, $Re_c = 19.8 \times 10^6$, low $q_\infty$.**



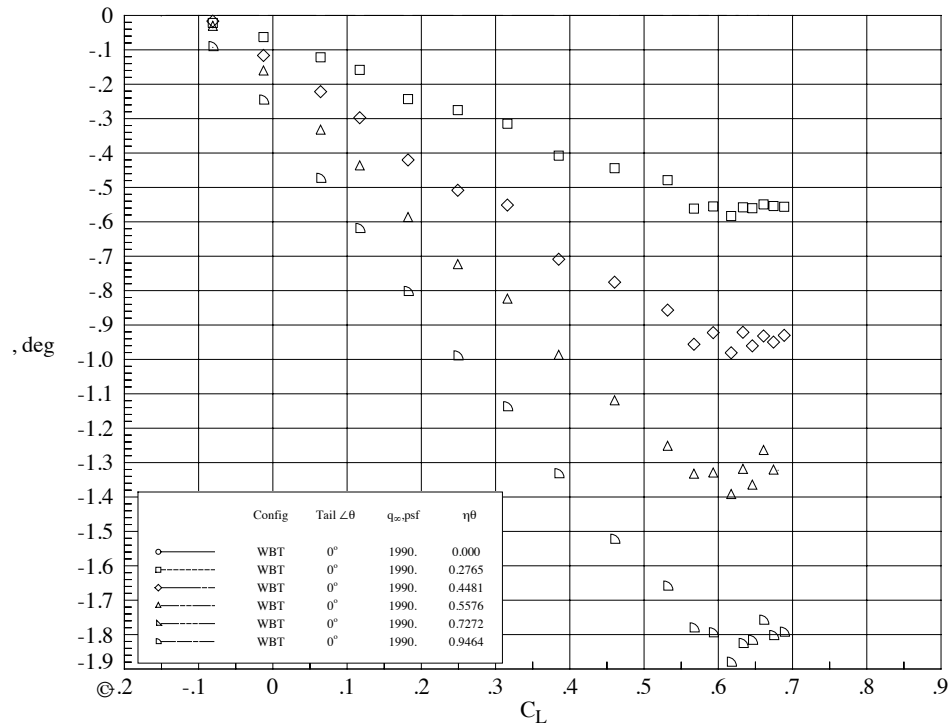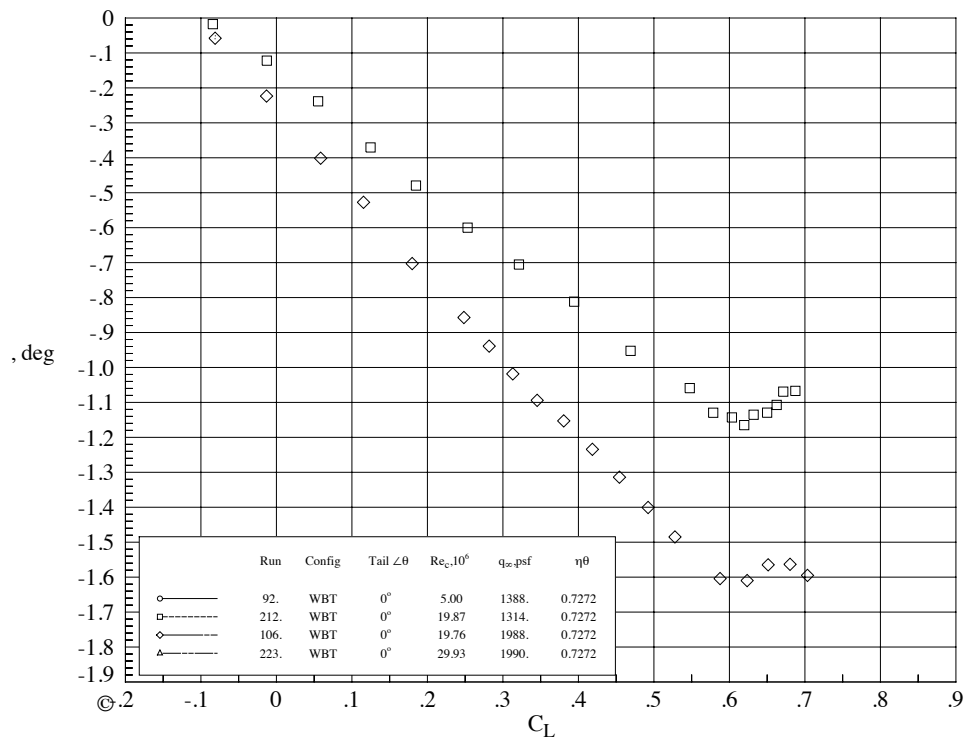**Figure 7. Model Deformation, WBT0 Configuration, Mach = 0.85, $Re_c = 19.8 \times 10^6$, high $q_\infty$.**

, deg

$C_L$

| | Config | Tail ∠θ | $q_\infty$,psf | ηθ |
|---|---|---|---|---|
| ○ | WBT | 0° | 1990. | 0.000 |
| □ | WBT | 0° | 1990. | 0.2765 |
| ◇ | WBT | 0° | 1990. | 0.4481 |
| △ | WBT | 0° | 1990. | 0.5576 |
| ◁ | WBT | 0° | 1990. | 0.7272 |
| ◁ | WBT | 0° | 1990. | 0.9464 |

**Figure 8. Model Deformation, WBT0 Configuration, Mach = 0.85, Re$_c$ = 30x10$^6$, high q$_\infty$.**

, deg

$C_L$

| | Run | Config | Tail ∠θ | Re$_c$.10$^6$ | $q_\infty$.psf | ηθ |
|---|---|---|---|---|---|---|
| ○ | 92. | WBT | 0° | 5.00 | 1388. | 0.7272 |
| □ | 212. | WBT | 0° | 19.87 | 1314. | 0.7272 |
| ◇ | 106. | WBT | 0° | 19.76 | 1988. | 0.7272 |
| △ | 223. | WBT | 0° | 29.93 | 1990. | 0.7272 |

**Figure 9. Model Deformation, WBT0 Configuration, Mach = 0.85, η = 0.7272.**

| | Run | Config | Tail ∠θ | $Re_c.10^6$ | $q_\infty.psf$ | ηθ |
|---|---|---|---|---|---|---|
| ○——— | 44. | WB | off | 4.99 | 1388. | 0.7272 |
| □--------- | 250. | WB | off | 19.84 | 1313. | 0.7272 |
| ◇— - — | 159. | WB | off | 19.76 | 1988. | 0.7272 |
| △------- | 146. | WB | off | 29.92 | 1989. | 0.7272 |
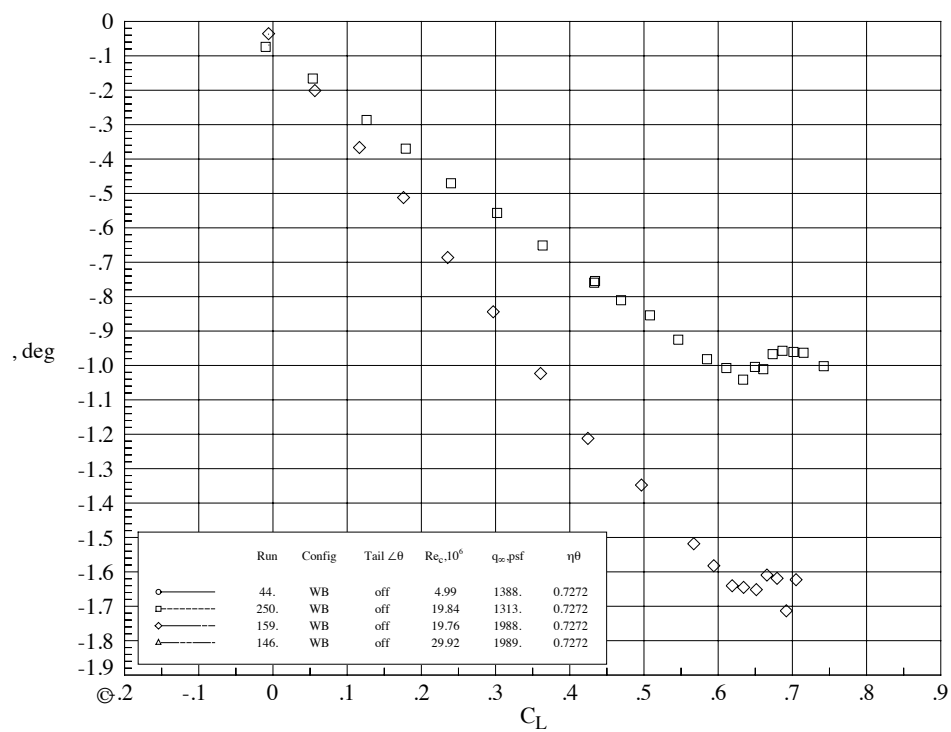
**Figure 10. Model Deformation, WB Configuration, Mach = 0.85, η = 0.7272.**

American Institute of Aeronautics and Astronautics

| | Run | Config | Tail | $M_{\infty\angle}$ | $Re_c,10^6$ | $q_{\infty},psf$ |
|---|---|---|---|---|---|---|
| ○——— | 247. | WB | off | 0.70 | 19.8 | 1150. |
| □------- | 156. | WB | off | 0.70 | 19.8 | 1740. |
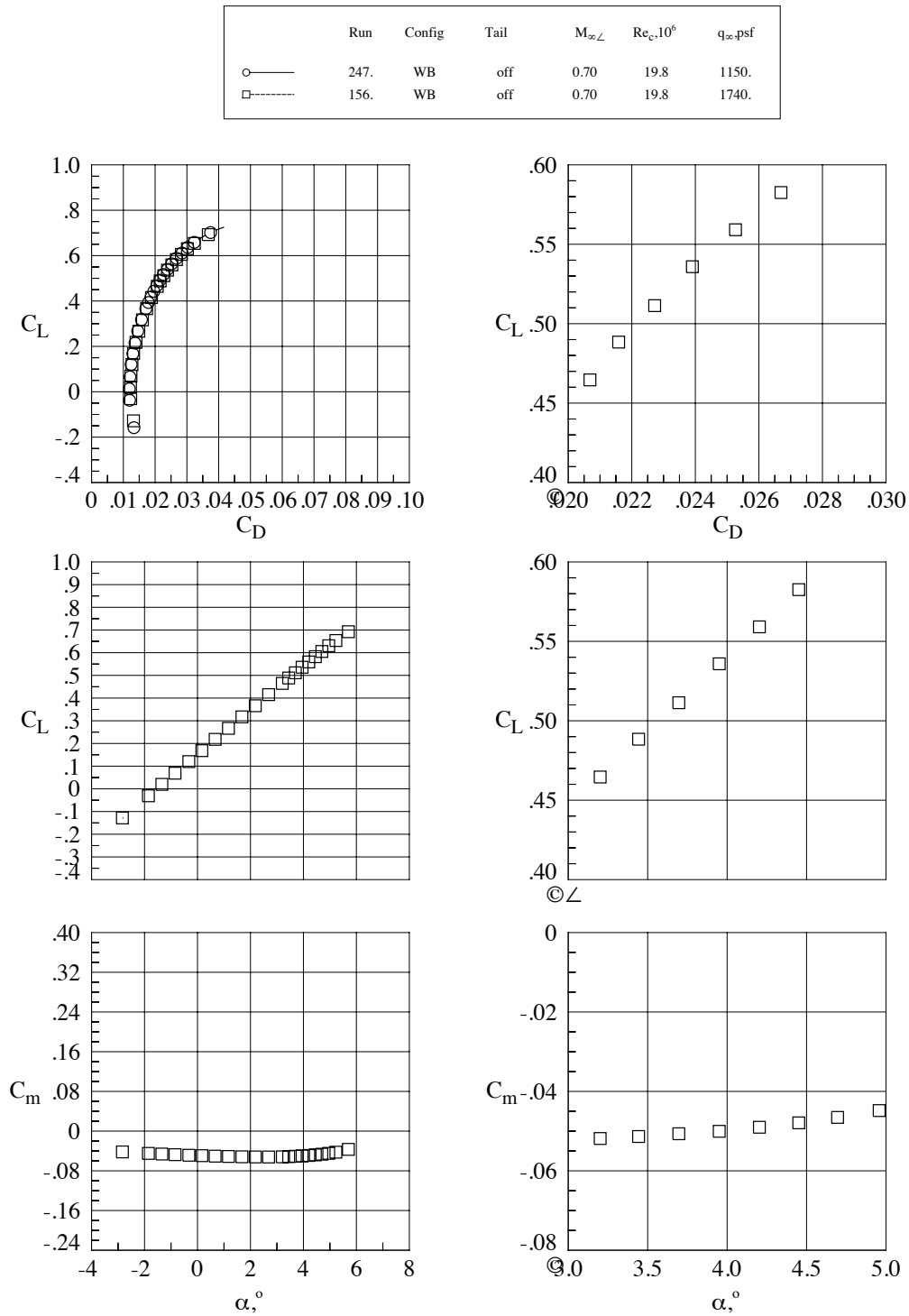


**Figure 11. Aeroelastic effects, WB Configuration, Mach = 0.7, $Re_c$ = 19.8x10^{6}.**

| | Run | Config | Tail | $M_{\infty\angle}$ | $Re_c, 10^6$ | $q_{\infty}$, psf |
|---|---|---|---|---|---|---|
| o——— | 209. | WBT | 0° | 0.70 | 19.8 | 1150. |
| □------- | 103. | WBT | 0° | 0.70 | 19.8 | 1740. |
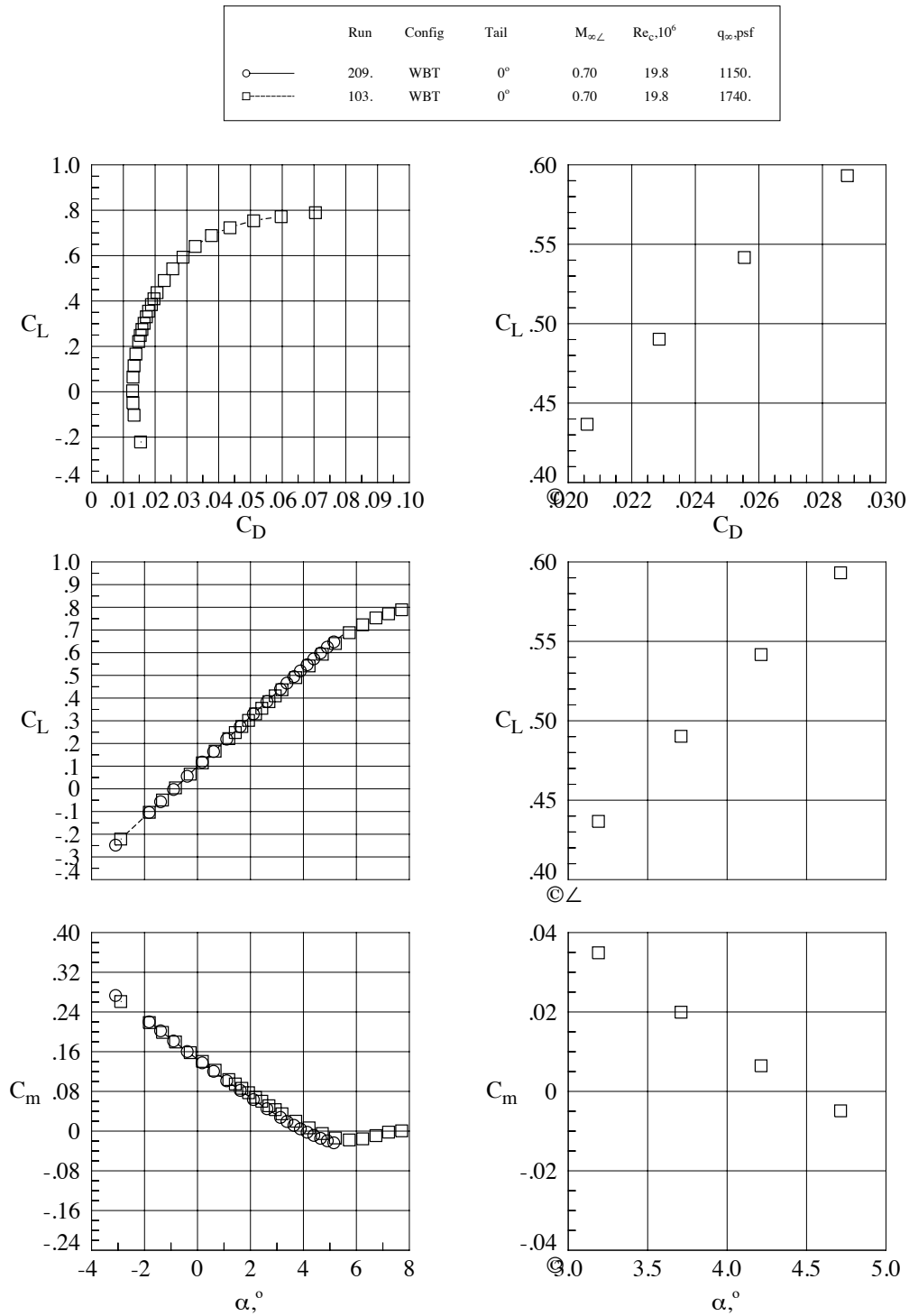
**Figure 12. Aeroelastic effects, WBT0 Configuration, Mach = 0.7, $Re_c$ = 19.8x10^{6}.**

15
American Institute of Aeronautics and Astronautics

| | Run | Config | Tail | $M_{\infty\angle}$ | $Re_c, 10^6$ | $q_{\infty}, psf$ |
|---|---|---|---|---|---|---|
| ○——— | 250. | WB | off | 0.85 | 19.8 | 1313. |
| □------- | 159. | WB | off | 0.85 | 19.8 | 1988. |
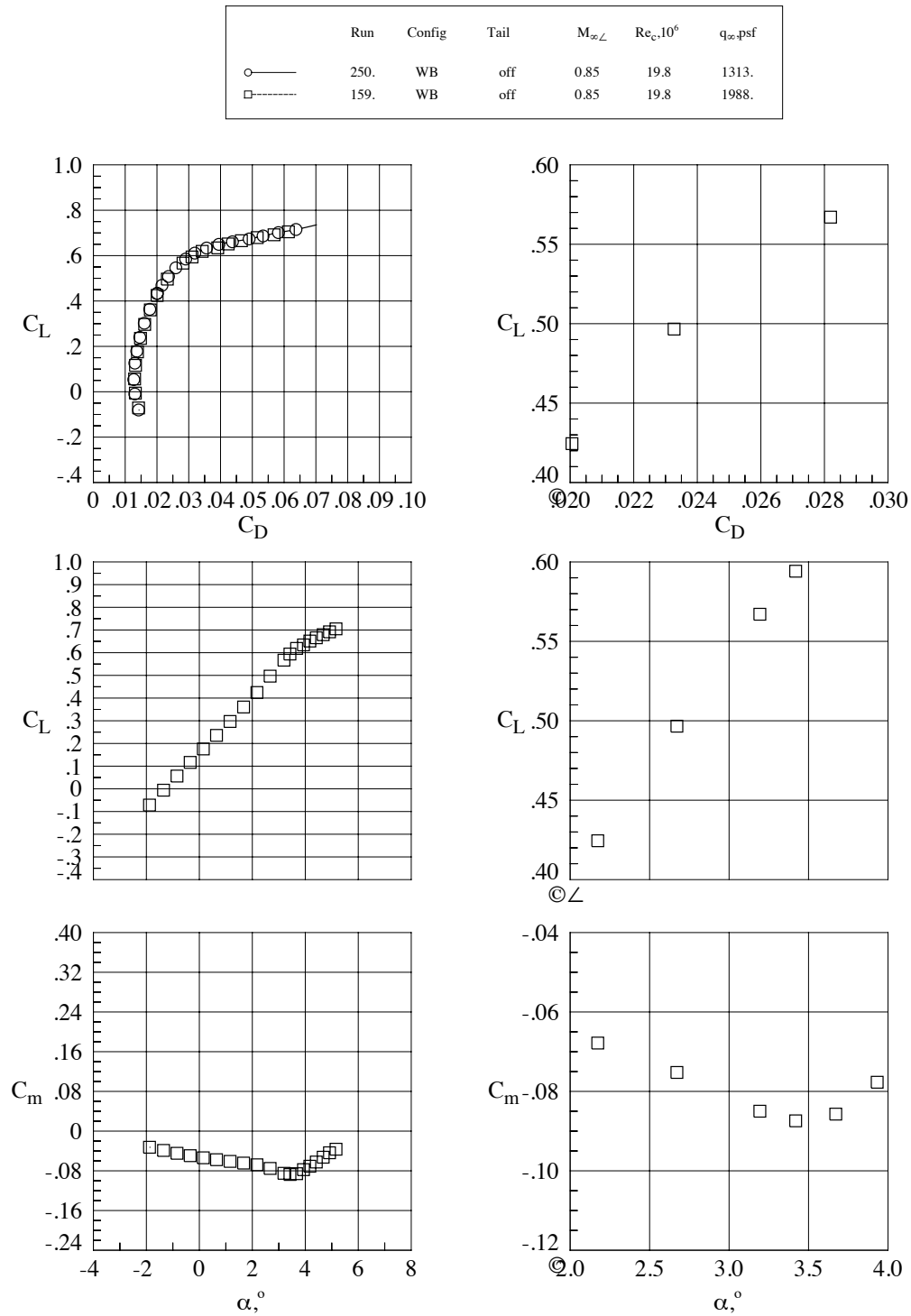


**Figure 13. Aeroelastic effects, WB Configuration, Mach = 0.85, $Re_c = 19.8 \times 10^6$.**

| | Run | Config | Tail | $M_{\infty\angle}$ | $Re_c,10^6$ | $q_{\infty}$,psf |
|---|---|---|---|---|---|---|
| ○——— | 212. | WBT | 0° | 0.85 | 19.9 | 1314. |
| □------- | 106. | WBT | 0° | 0.85 | 19.8 | 1988. |
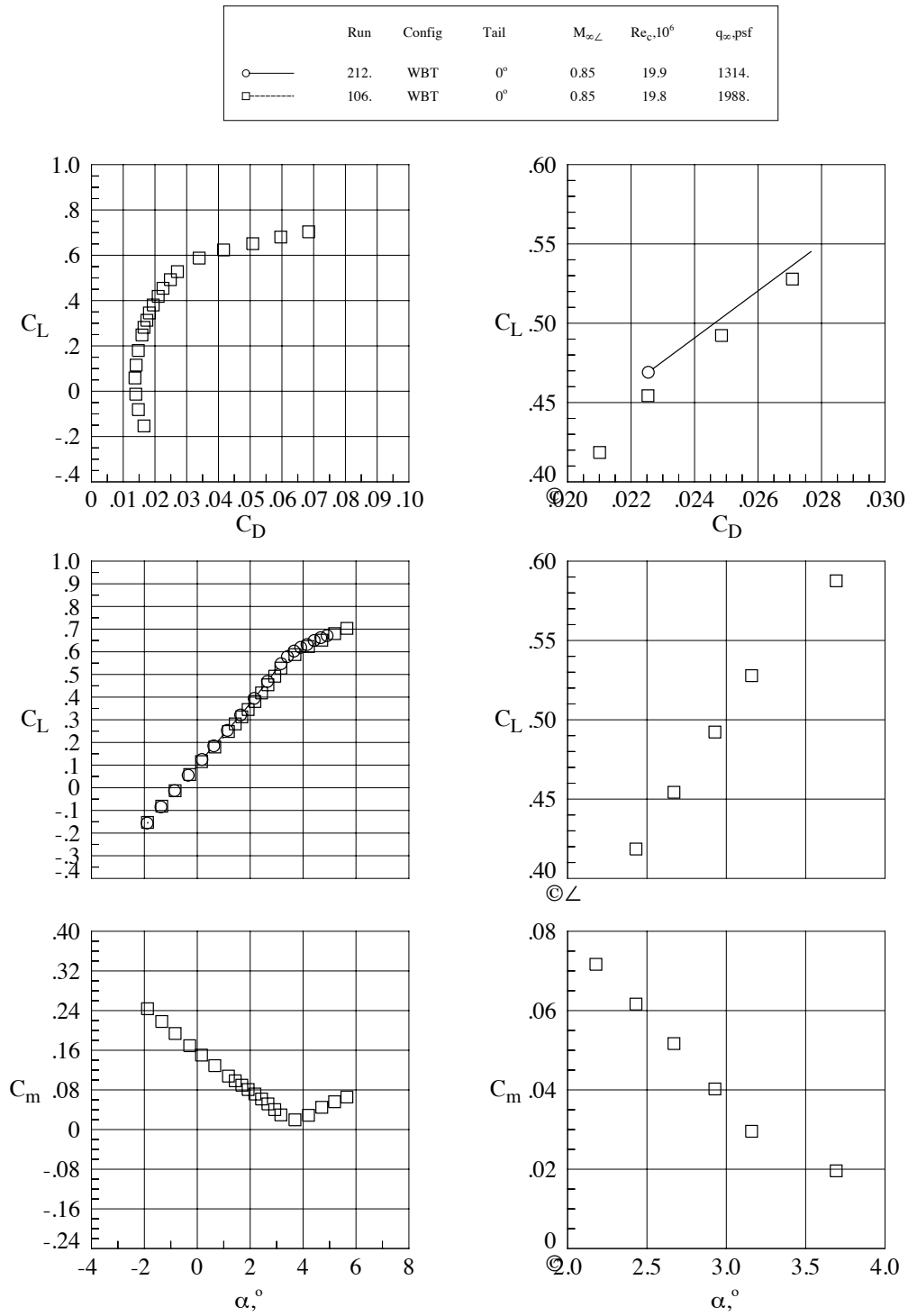


**Figure 14. Aeroelastic effects, WBT0 Configuration, Mach = 0.85, $Re_c$ = 19.8x10^{6}.**

American Institute of Aeronautics and Astronautics

| | Run | Config | Tail | $M_{\infty\angle}$ | $Re_c, 10^6$ | $q_\infty$, psf |
|---|---|---|---|---|---|---|
| ○——— | 251. | WB | off | 0.87 | 19.9 | 1333. |
| □------- | 160. | WB | off | 0.87 | 19.8 | 2018. |
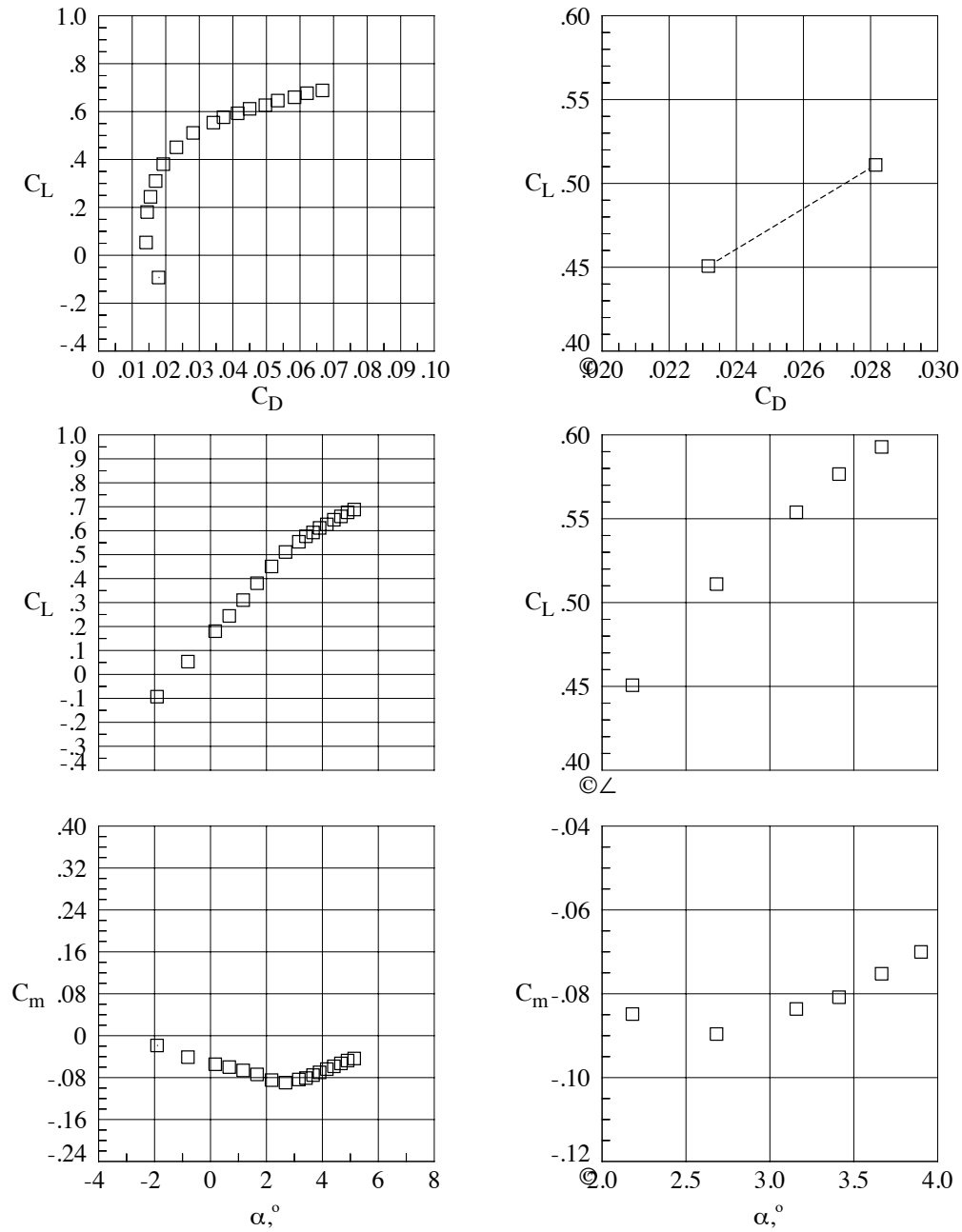
**Figure 15. Aeroelastic effects, WB Configuration, Mach = 0.87, $Re_c$ = 19.8x10$^6$.**

| | Run | Config | Tail | $M_{\infty\angle}$ | $Re_c,10^6$ | $q_\infty$,psf |
|---|---|---|---|---|---|---|
| ○——— | 213. | WBT | 0° | 0.87 | 19.9 | 1333. |
| □------- | 107. | WBT | 0° | 0.87 | 19.8 | 2017. |
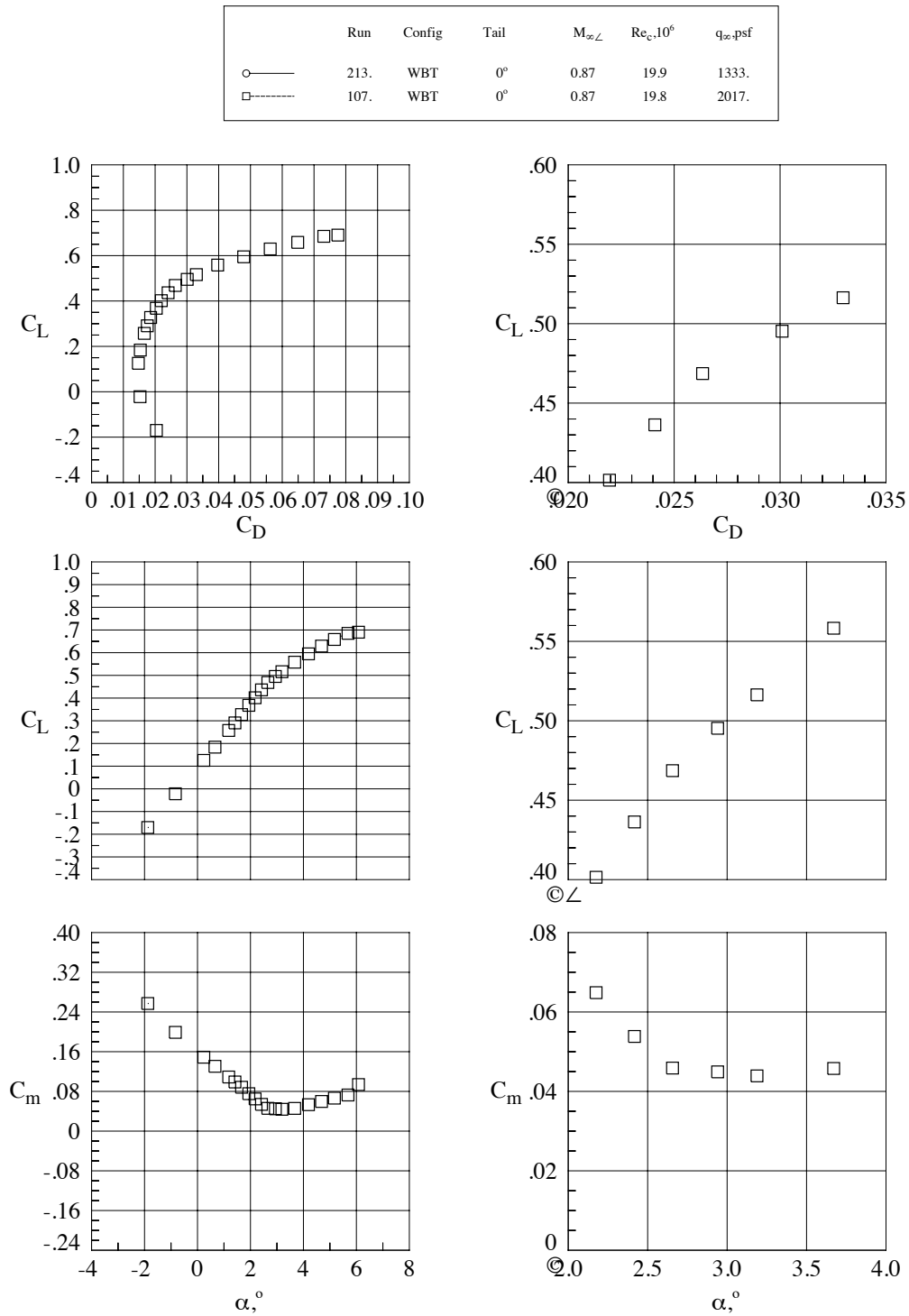


**Figure 16. Aeroelastic effects, WBT0 Configuration, Mach = 0.87, $Re_c = 19.8 \times 10^6$.**

| | Run | Config | $M_\infty$ | $Re_c, 10^6$ | $q_\infty$, psf |
|---|---|---|---|---|---|
| ○——— | 39. | WB | 0.70 | 5.0 | 1205. |
| □-------- | 69. | WBPN | 0.70 | 5.0 | 1205. |
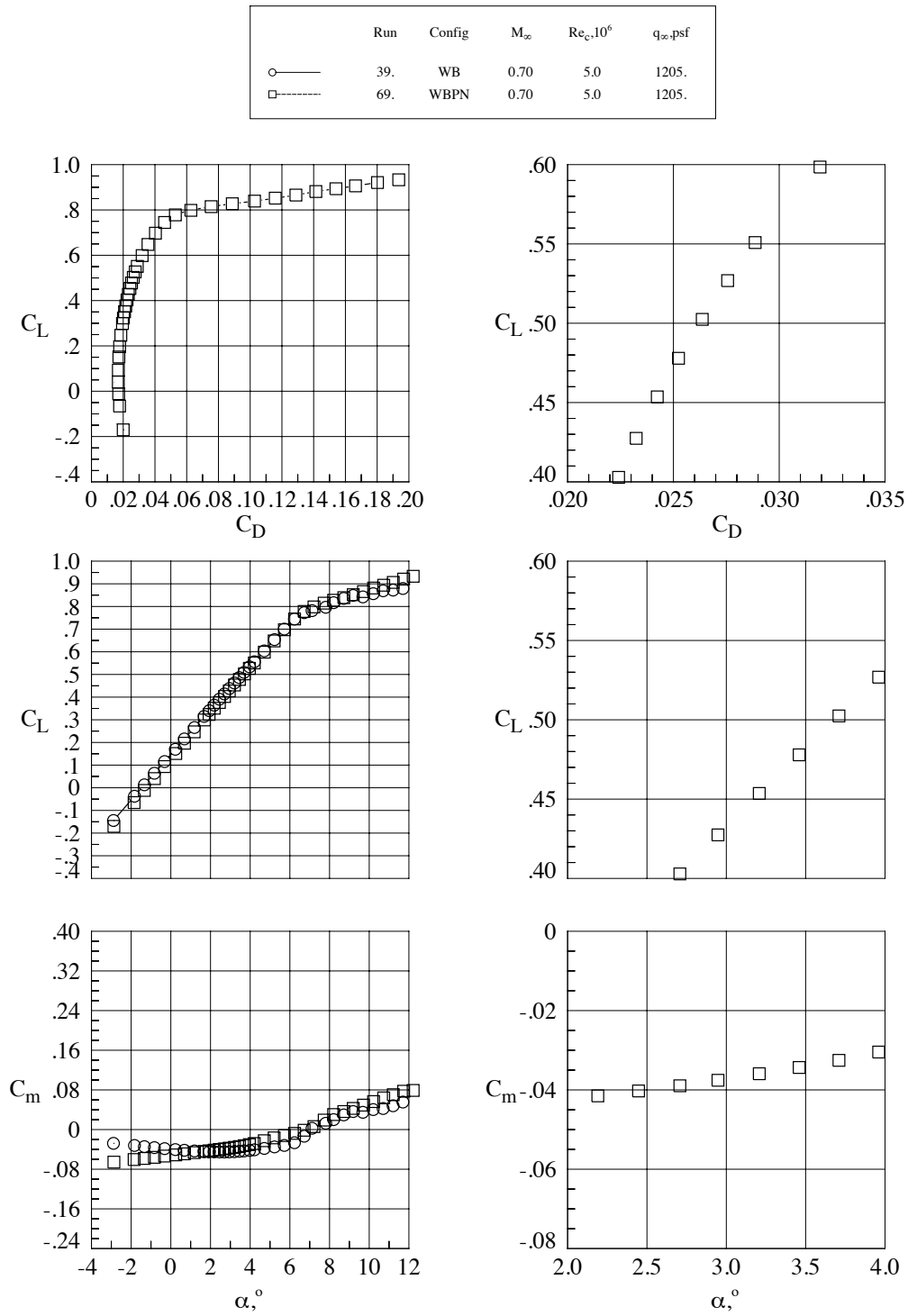
**Figure 17. Nacelle/Pylon effects, Mach = 0.7, $Re_c = 5 \times 10^6$.**

| | | Run | Config | M | $Re_c, 10^6$ | q ,psf |
|---|---|---|---|---|---|---|
| ○ | —— | 44. | WB | 0.85 | 5.0 | 1388. |
| □ | ------- | 74. | WBPN | 0.85 | 5.0 | 1388. |
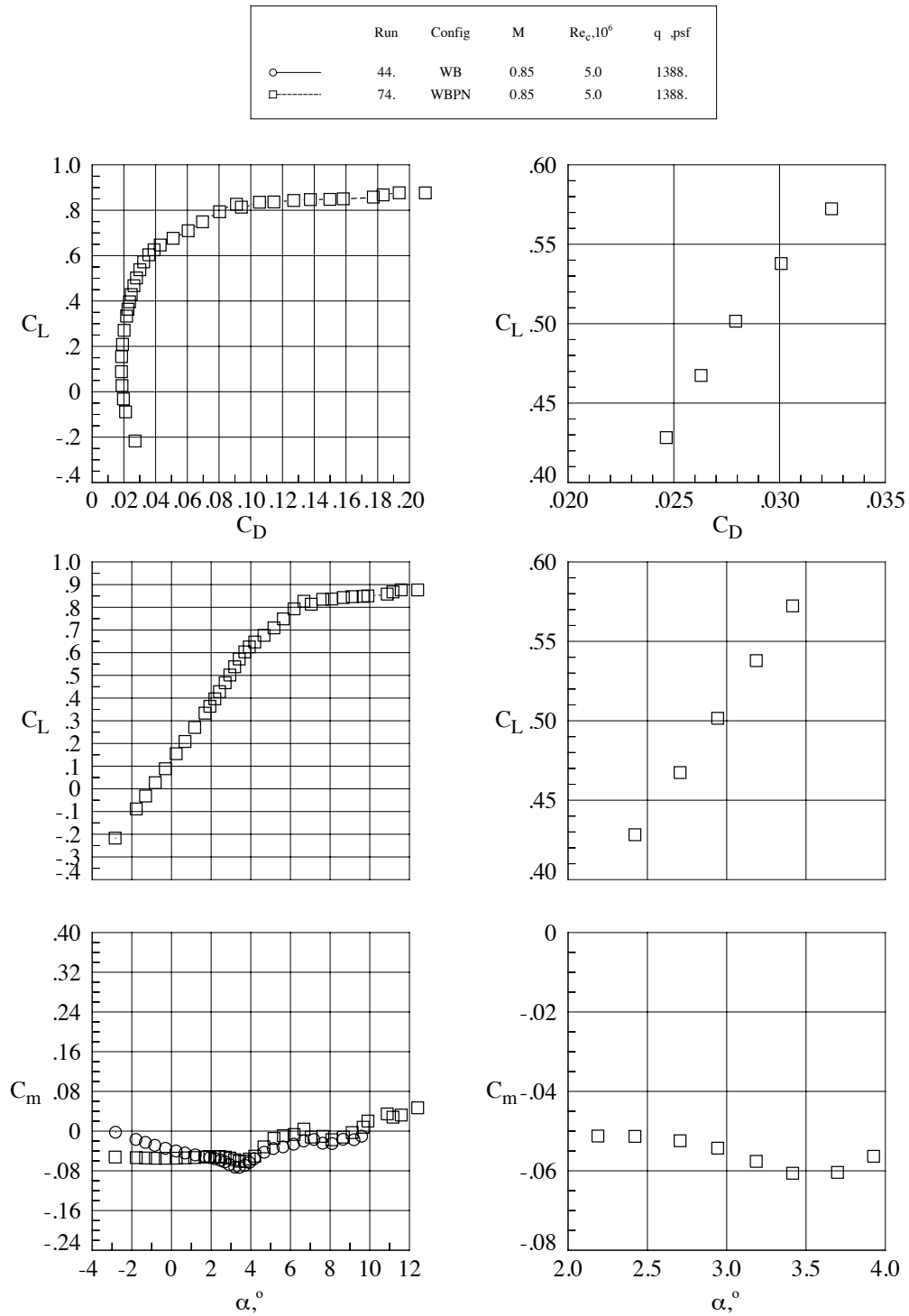
**Figure 18. Nacelle/Pylon Effects, Mach = 0.85, $Re_c = 5x10^6$.**

American Institute of Aeronautics and Astronautics

| | Run | Config | M | $Re_c, 10^6$ | q ,psf |
|---|---|---|---|---|---|
| ○——— | 47. | WB | 0.87 | 5.0 | 1410. |
| □------ | 77. | WBPN | 0.87 | 5.0 | 1410. |
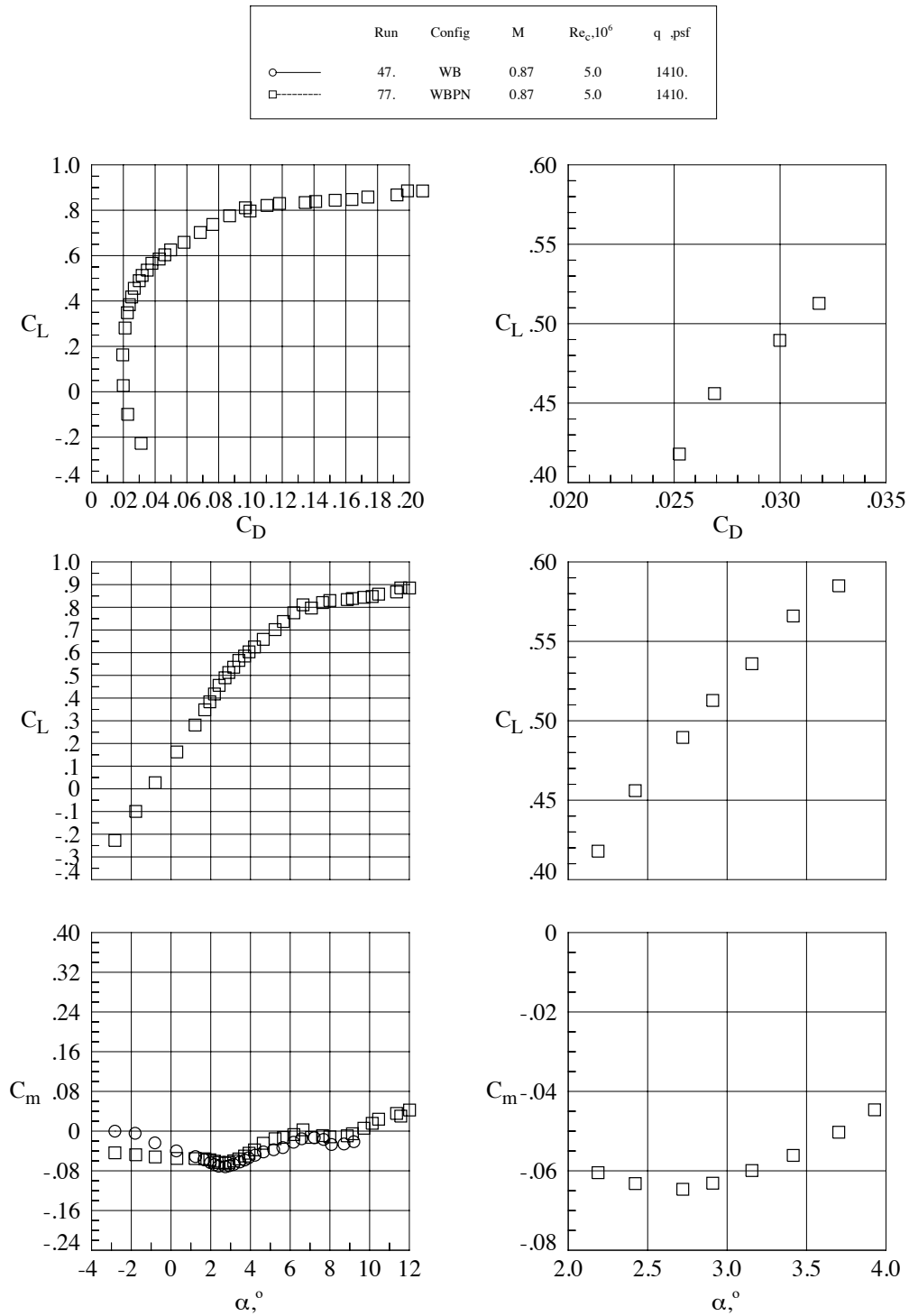
**Figure 19. Nacelle/Pylon Effects, Mach = 0.87, $Re_c = 5 \times 10^6$.**

American Institute of Aeronautics and Astronautics

| | Run | Config | Tail | $M_{\infty\angle}$ | $Re_c, 10^6$ | $q_{\infty}, psf$ |
|---|---|---|---|---|---|---|
| ○——— | 39. | WB | off | 0.70 | 5.0 | 1205. |
| □-------- | 247. | WB | off | 0.70 | 19.8 | 1150. |
| ◇— — | 156. | WB | off | 0.70 | 19.8 | 1740. |
| △——·—— | 143. | WB | off | 0.70 | 30.0 | 1743. |
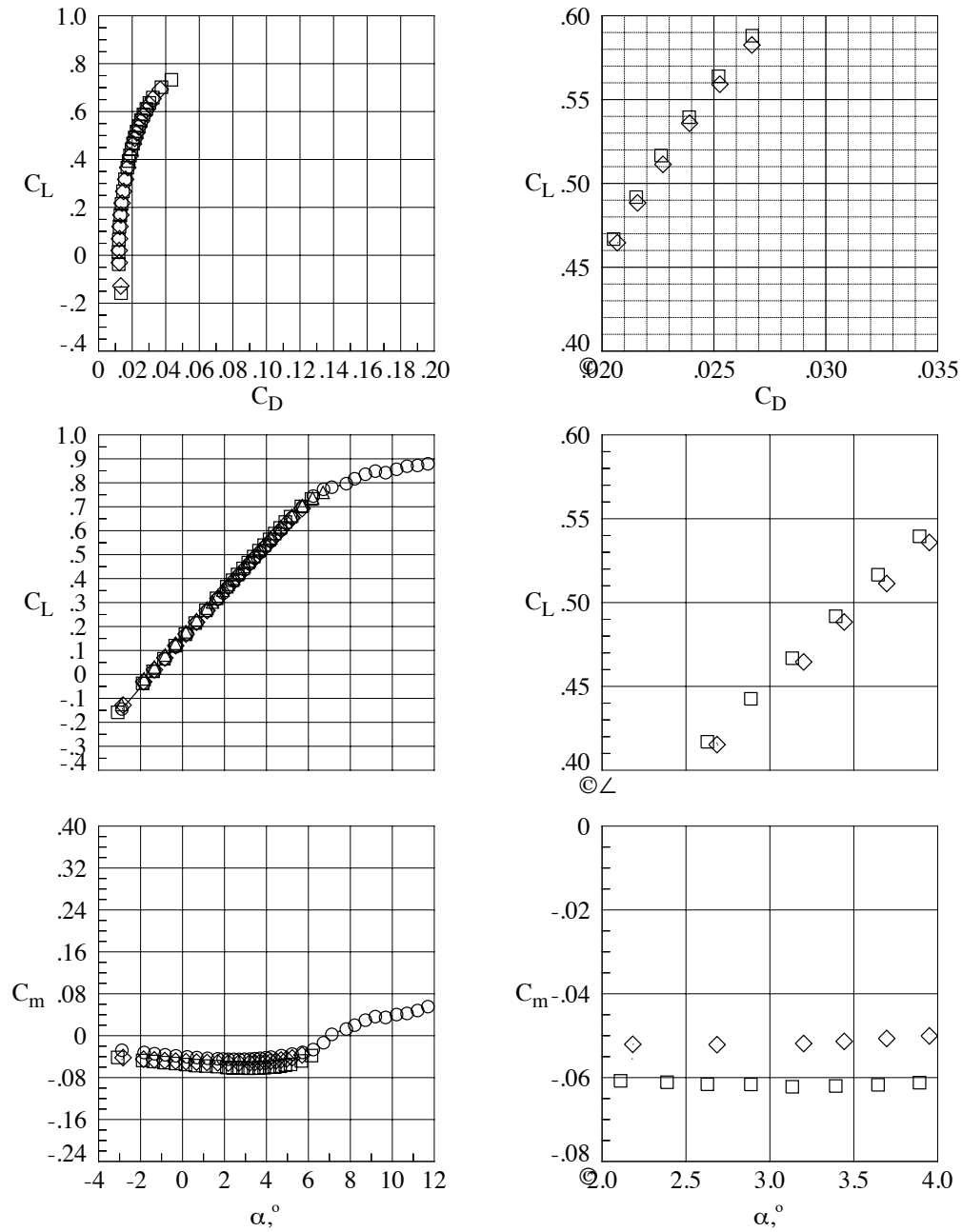
**Figure 20. Reynolds Number Effects, WB Configuration, Mach = 0.7.**

American Institute of Aeronautics and Astronautics

| | Run | Config | Tail | $M_{\infty\perp}$ | $Re_c, 10^6$ | $q_\infty$, psf |
|---|---|---|---|---|---|---|
| ○——— | 87. | WBT | 0° | 0.70 | 5.0 | 1205. |
| □------- | 209. | WBT | 0° | 0.70 | 19.8 | 1150. |
| ◇— - — | 103. | WBT | 0° | 0.70 | 19.8 | 1740. |
| △— - - — | 220. | WBT | 0° | 0.70 | 30.0 | 1743. |
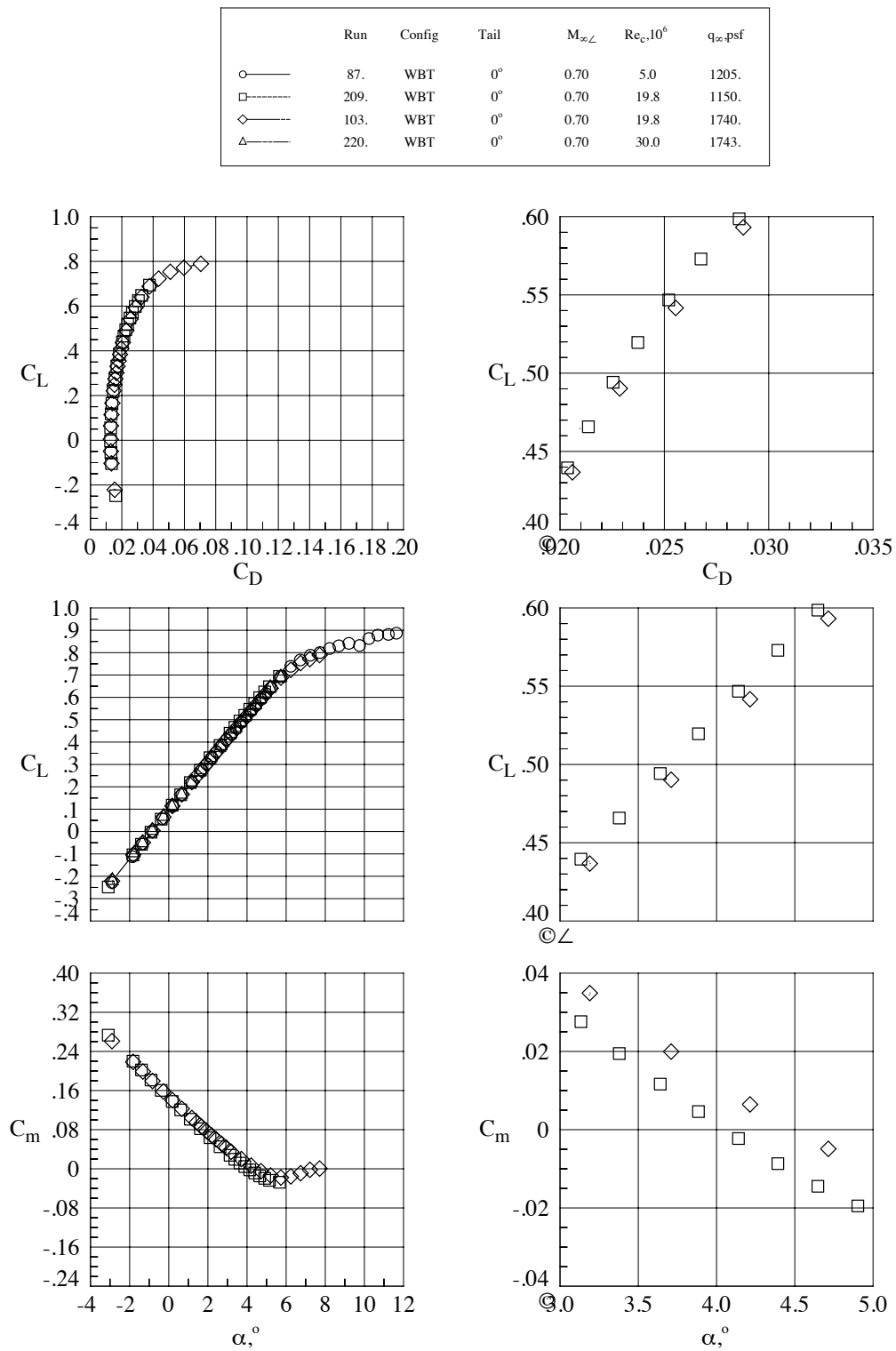
**Figure 21. Reynolds Number Effects, WBT0 Configuration, Mach = 0.7.**

24

American Institute of Aeronautics and Astronautics

| | Run | Config | Tail | $M_{\infty\angle}$ | $Re_c, 10^6$ | $q_{\infty},$ psf |
|---|---|---|---|---|---|---|
| ○——— | 44. | WB | off | 0.85 | 5.0 | 1388. |
| □------- | 250. | WB | off | 0.85 | 19.8 | 1313. |
| ◇—·—· | 159. | WB | off | 0.85 | 19.8 | 1988. |
| △—··—·· | 146. | WB | off | 0.85 | 29.9 | 1989. |
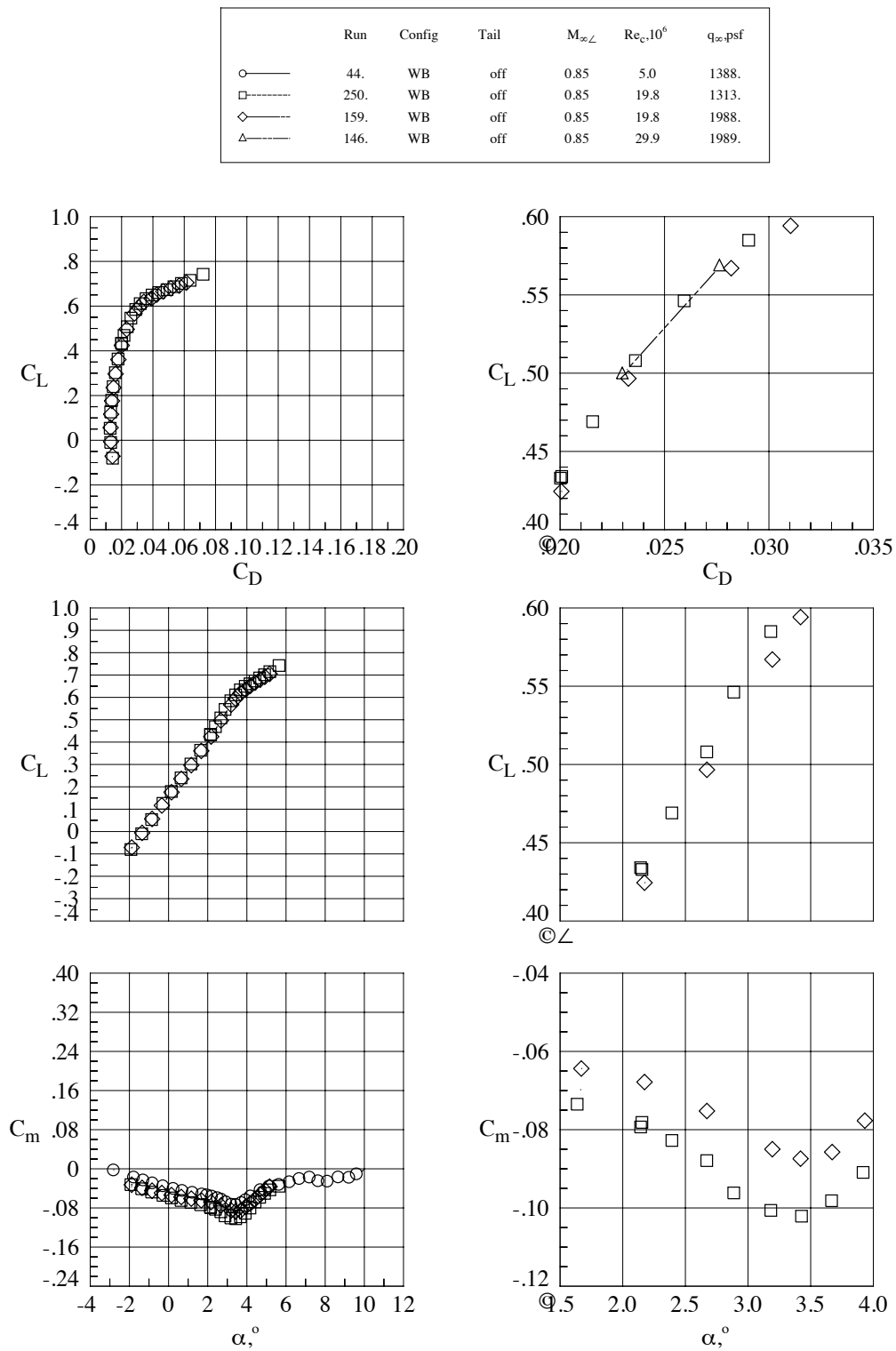
**Figure 22. Reynolds Number Effects, WB Configuration, Mach = 0.85.**

American Institute of Aeronautics and Astronautics

| | Run | Config | Tail | $M_{\infty\angle}$ | $Re_c,10^6$ | $q_\infty$,psf |
|---|---|---|---|---|---|---|
| ○——— | 92. | WBT | 0° | 0.85 | 5.0 | 1388. |
| □-------- | 212. | WBT | 0° | 0.85 | 19.9 | 1314. |
| ◇--·-- | 106. | WBT | 0° | 0.85 | 19.8 | 1988. |
| △--·--- | 223. | WBT | 0° | 0.85 | 29.9 | 1990. |
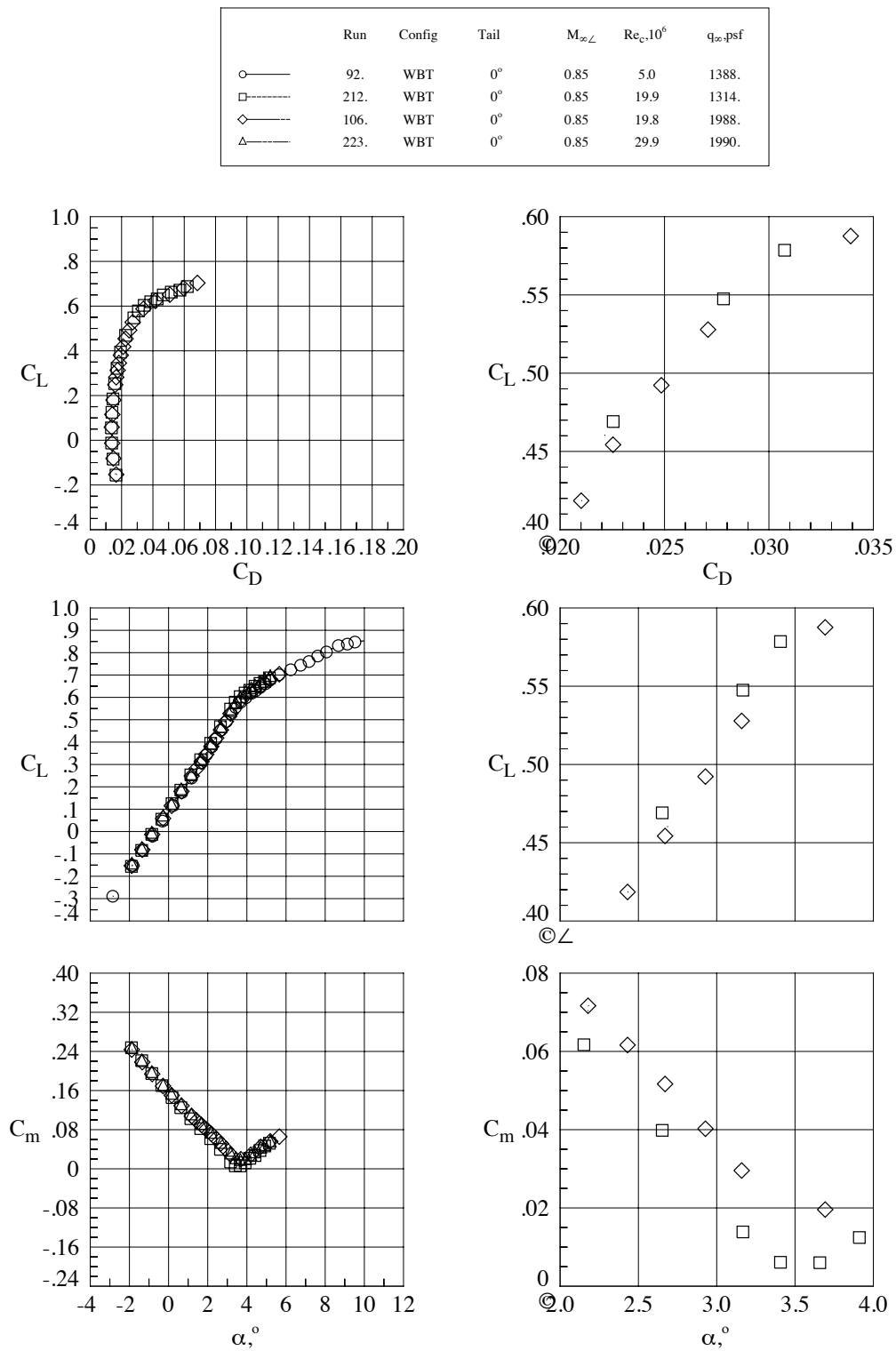
**Figure 23. Reynolds Number Effects, WBT0 Configuration, Mach = 0.85.**

| | Run | Config | Tail | $M_{\infty\angle}$ | $Re_c, 10^6$ | $q_\infty$, psf |
|---|---|---|---|---|---|---|
| ○——— | 47. | WB | off | 0.87 | 5.0 | 1410. |
| □------- | 251. | WB | off | 0.87 | 19.9 | 1333. |
| ◇—·— | 160. | WB | off | 0.87 | 19.8 | 2018. |
| △—··— | 147. | WB | off | 0.87 | 29.9 | 2019. |
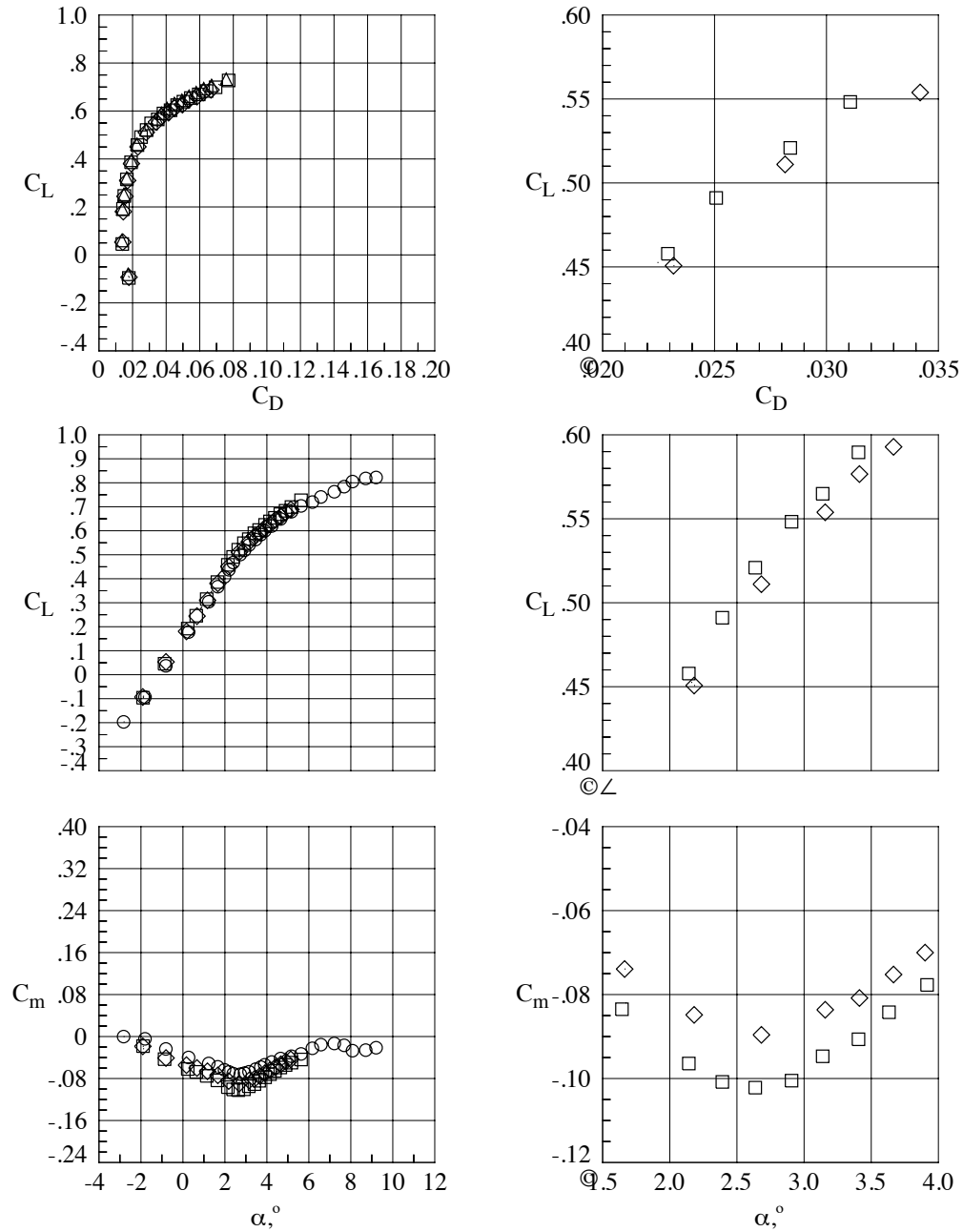


Figure 24. Reynolds Number Effects, WB Configuration, Mach = 0.87.

| | Run | Config | Tail | $M_{\infty\angle}$ | $Re_c, 10^6$ | $q_\infty$, psf |
|---|---|---|---|---|---|---|
| ○——— | 95. | WBT | 0° | 0.87 | 5.0 | 1410. |
| □--------- | 213. | WBT | 0° | 0.87 | 19.9 | 1333. |
| ◇— —— | 107. | WBT | 0° | 0.87 | 19.8 | 2017. |
| △——·——· | 224. | WBT | 0° | 0.87 | 29.9 | 2019. |
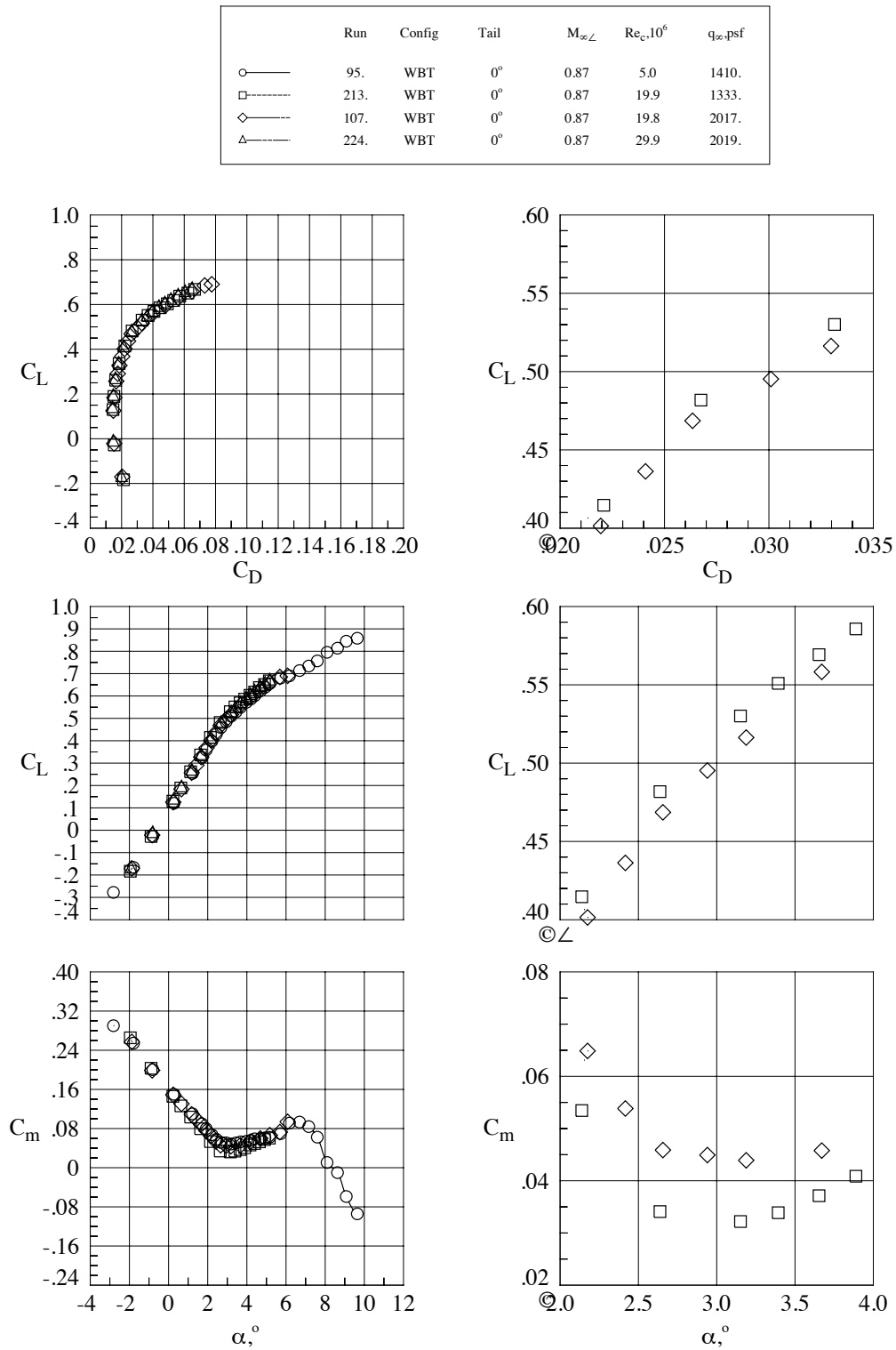
**Figure 25. Reynolds Number Effects, WBT0 Configuration, Mach = 0.87.**

| | Run | Config | Tail | $M_{\infty \angle}$ | $Re_c, 10^6$ | $q_\infty$, psf |
|---|---|---|---|---|---|---|
| ○——— | 39. | WB | off | 0.70 | 5.0 | 1205. |
| □------- | 192. | WBT | -2° | 0.70 | 5.0 | 1205. |
| ◇— · — | 87. | WBT | 0° | 0.70 | 5.0 | 1205. |
| △— · · — | 173. | WBT | +2° | 0.70 | 5.0 | 1205. |
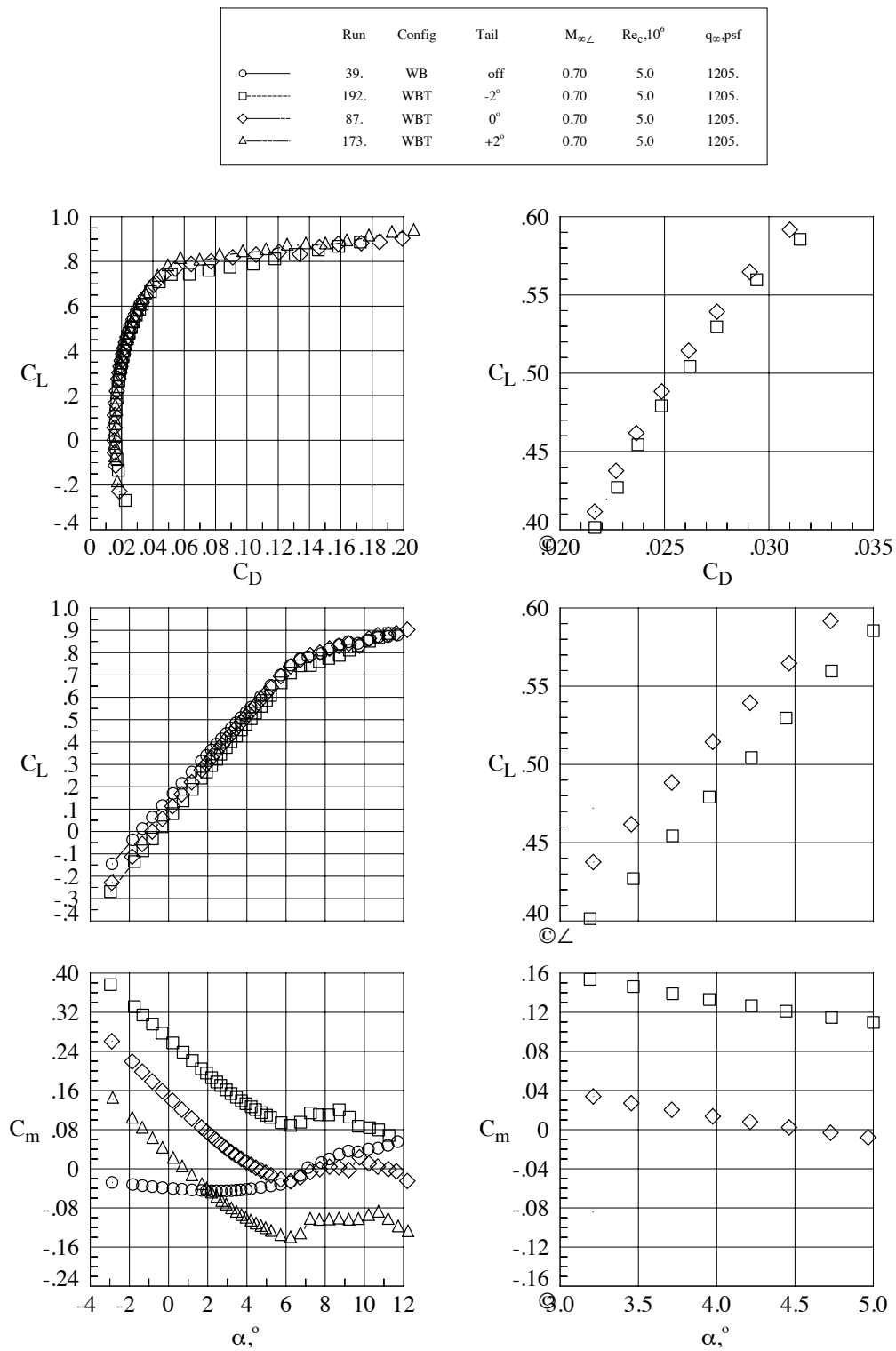
**Figure 26. Tail Effects, Mach = 0.7, $Re_c = 5 \times 10^6$.**

| | Run | Config | Tail | $M_\infty$ | $Re_c, 10^6$ | $q_\infty$, psf |
|---|---|---|---|---|---|---|
| ○——— | 44. | WB | off | 0.85 | 5.0 | 1388. |
| □------ | 196. | WBT | -2° | 0.85 | 5.0 | 1388. |
| ◇— ·— | 92. | WBT | 0° | 0.85 | 5.0 | 1388. |
| △—·—·— | 176. | WBT | +2° | 0.85 | 5.0 | 1388. |
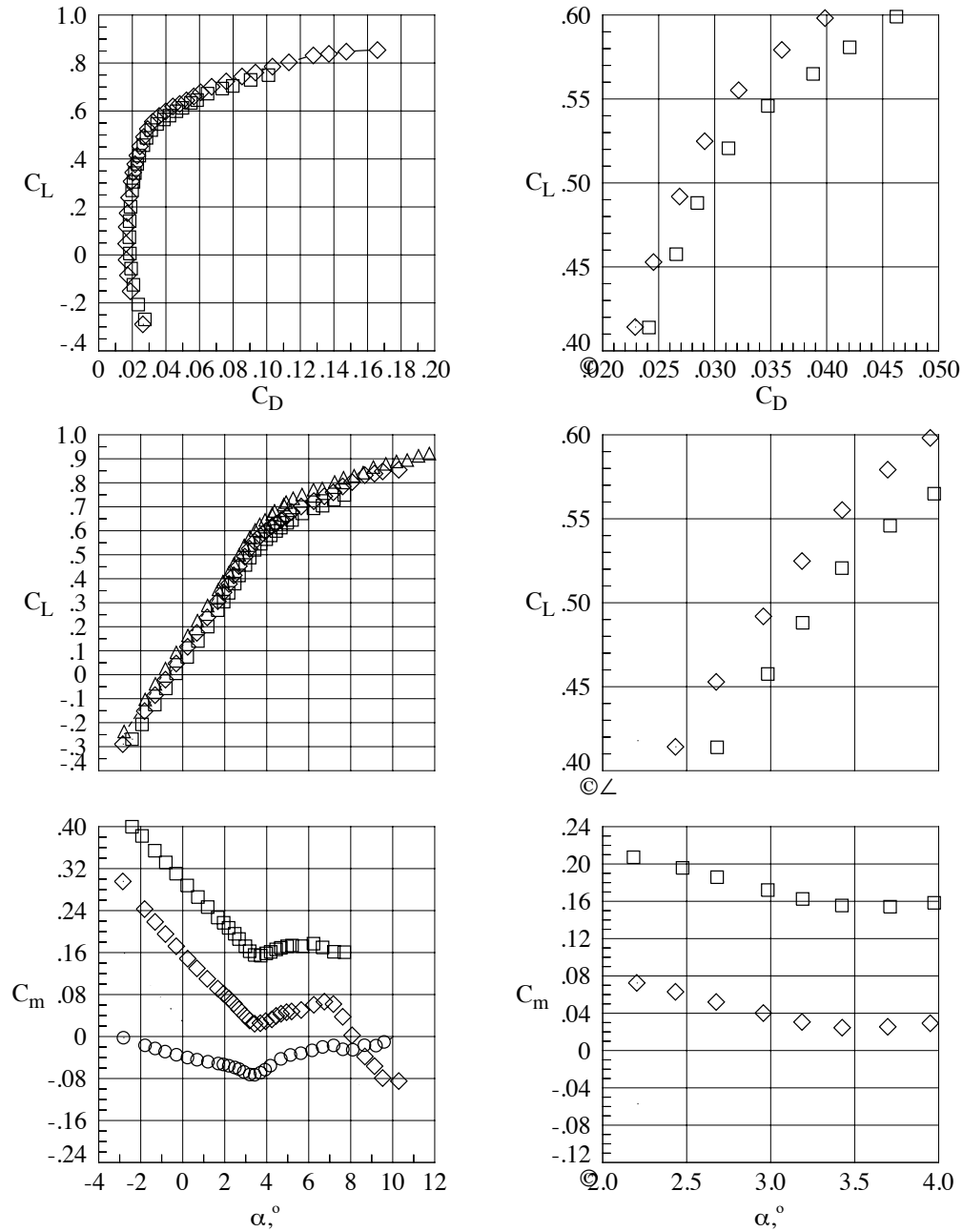
**Figure 27. Tail Effects, Mach = 0.85, $Re_c$ = 5x10$^6$.**

| | Run | Config | Tail | $M_{\infty\angle}$ | $Re_c,10^6$ | $q_\infty$,psf |
|---|---|---|---|---|---|---|
| ○——— | 47. | WB | off | 0.87 | 5.0 | 1410. |
| □------- | 198. | WBT | -2° | 0.87 | 5.0 | 1410. |
| ◇—·—· | 95. | WBT | 0° | 0.87 | 5.0 | 1410. |
| △—··—·· | 178. | WBT | +2° | 0.87 | 5.0 | 1410. |
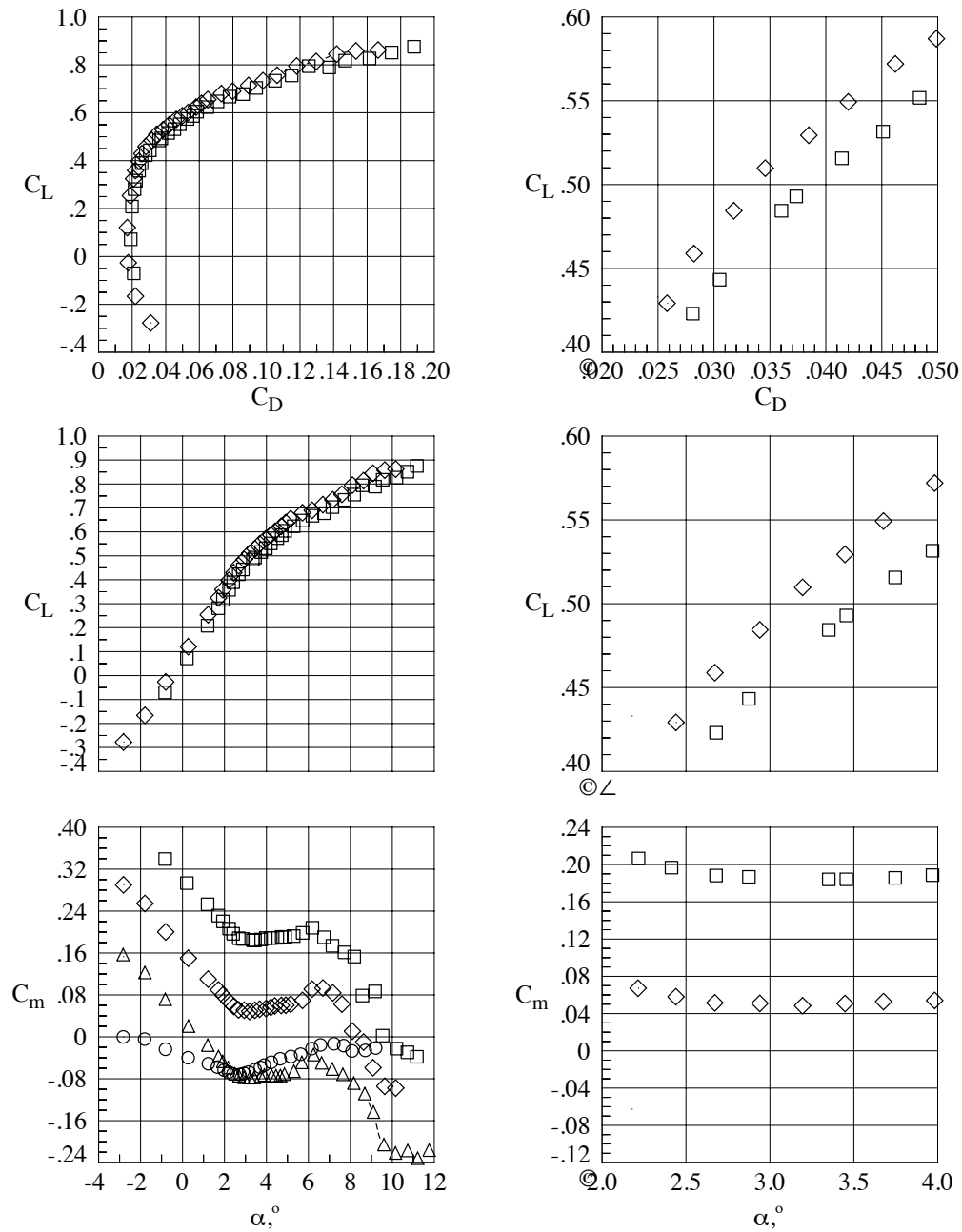


**Figure 28. Tail Effects, Mach = 0.87, $Re_c = 5x10^6$.**
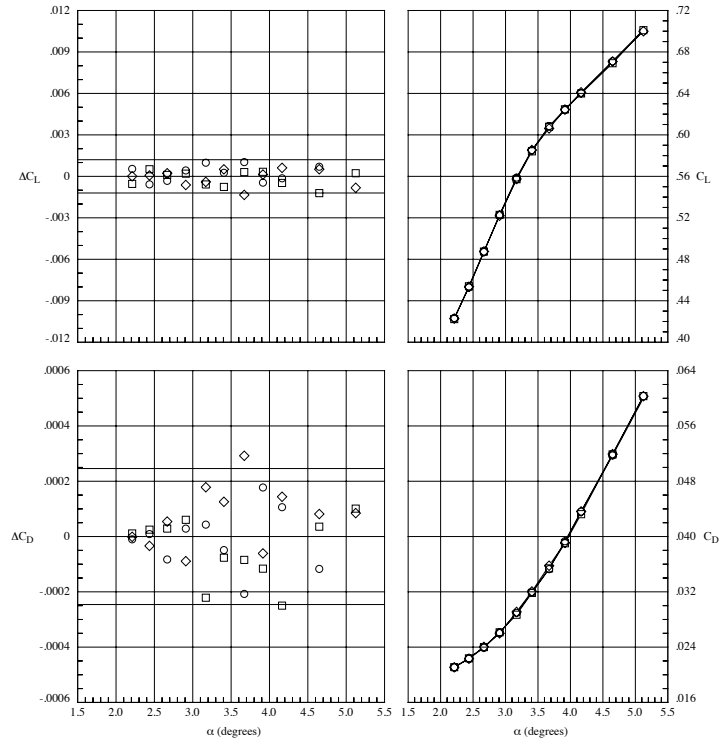
**Figure 29. Data Repeatability, WB Configuration, Mach = 0.85, $Re_c = 5 \times 10^6$.
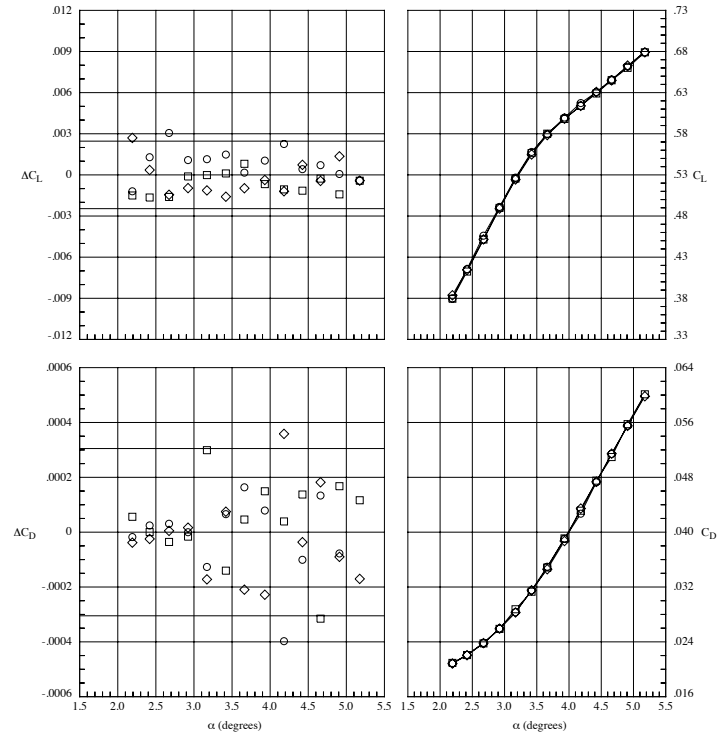Solid line indicates 2-sigma limits based on the residual data.**
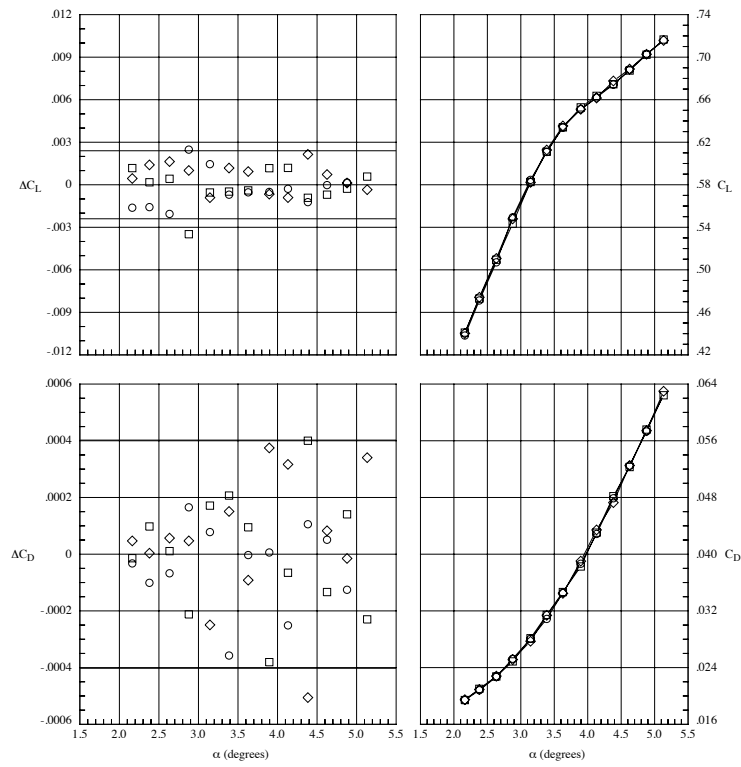


**Figure 30. Data Repeatability, WB Configuration, Mach = 0.85, $Re_c = 19.8 \times 10^6$.
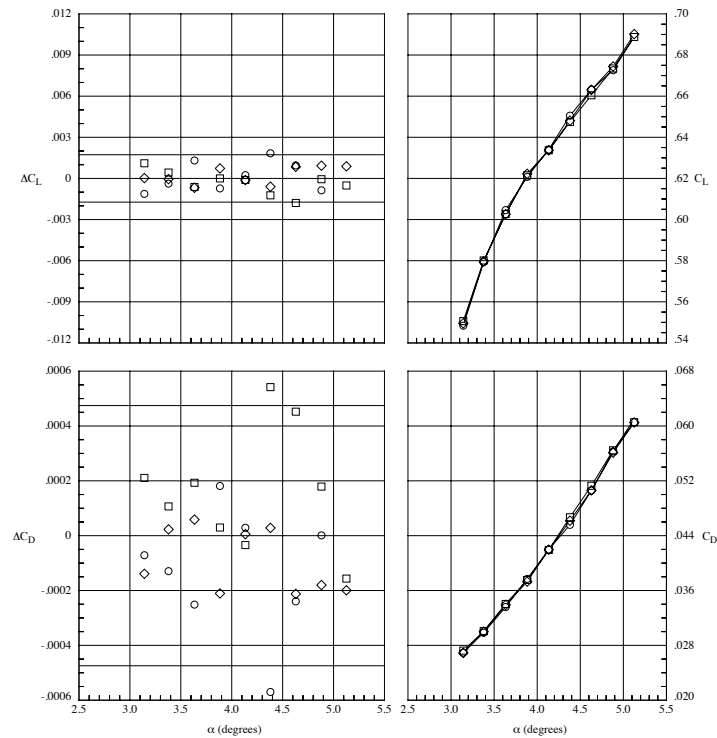Solid line indicates 2-sigma limits based on the residual data.**

American Institute of Aeronautics and Astronautics
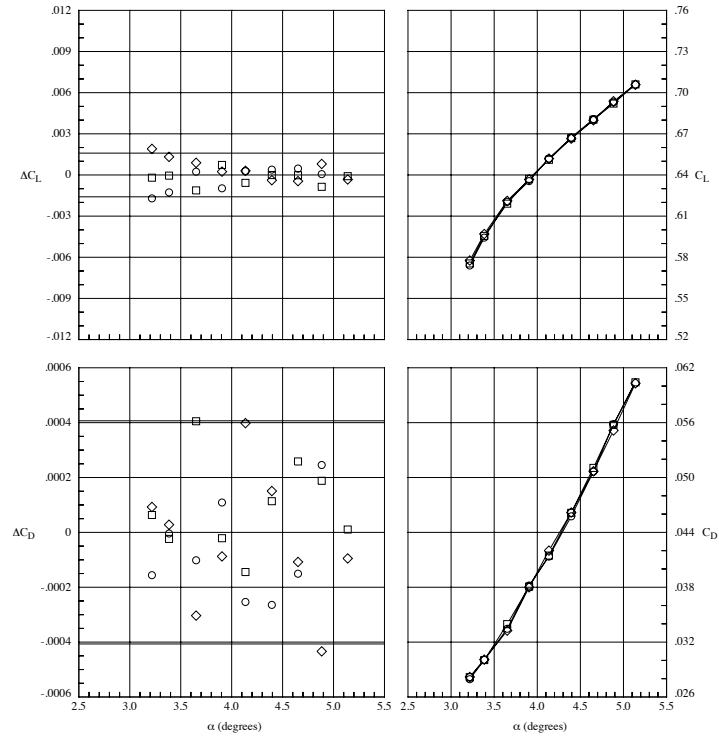
**Figure 31. Data Repeatability, WB Configuration, Mach = 0.85, $Re_c$ = 19.8x10^{6}.**
**Solid line indicates 2-sigma limits based on the residual data.**
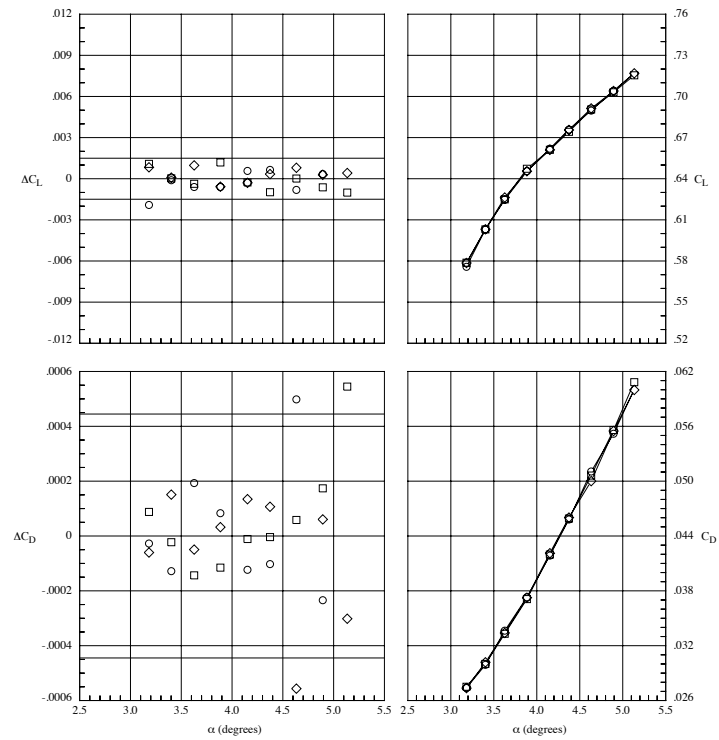


**Figure 32. Data Repeatability, WB Configuration, Mach = 0.85, $Re_c$ = 30x10^{6}.**
**Solid line indicates 2-sigma limits based on the residual data.**

American Institute of Aeronautics and Astronautics

**Figure 33. Data Repeatability, WBT0 Configuration, Mach = 0.85, $Re_c = 5 \times 10^6$.**
**Solid line indicates 2-sigma limits based on the residual data.**



**Figure 34. Data Repeatability, WBT0 Configuration, Mach = 0.85, $Re_c = 19.8 \times 10^6$.**
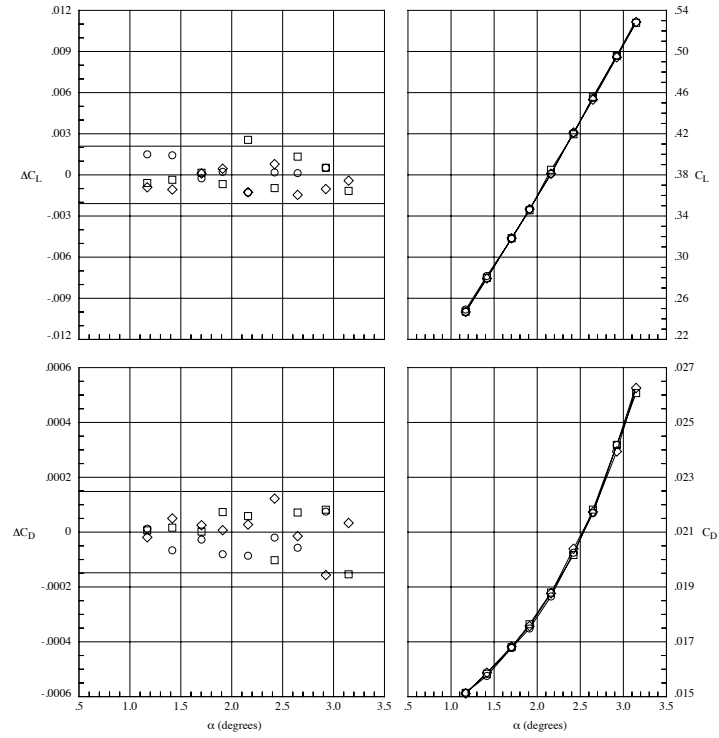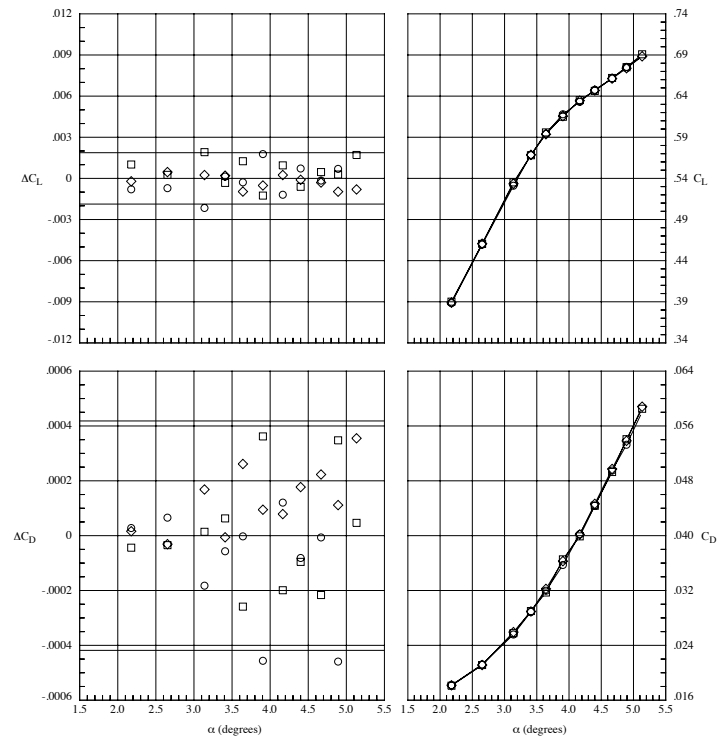**Solid line indicates 2-sigma limits based on the residual data.**

**Figure 35. Data Repeatability, WBT0 Configuration, Mach = 0.85, Re$_c$ = 19.8x10$^6$.
Solid line indicates 2-sigma limits based on the residual data.**



**Figure 36. Data Repeatability, WBT0 Configuration, Mach = 0.85, Re$_c$ = 30x10$^6$.
Solid line indicates 2-sigma limits based on the residual data.**

American Institute of Aeronautics and Astronautics